Journal of the Brazilian Society of Mechanical Sciences and Engineering (2026) 48:237
https://doi.org/10.1007/s40430-026-06315-8

TECHNICAL PAPER

Experimental investigation and multi-sensor based optimization of machining parameters considering vibration effects

Bayram Sercan Bayram[1] · **Mehmet Okan Kabakçı**[1] · **İbrahim Baki Şahin**[2] · **İhsan Korkut**[1]

Received: 29 July 2025 / Accepted: 4 January 2026 / Published online: 3 March 2026

Abstract

In this study, a multi-objective optimization of AA7075-T6 machining performance was conducted using data from cutting force, vibration, power consumption, and surface roughness. A hybrid Taguchi–GRA–CRITIC optimization model was employed to evaluate and optimize multiple performance criteria objectively. Additionally, the effects of vibration on surface integrity were examined through Power Spectral Density (PSD) and Short-Time Fourier Transform (STFT) analyses. The optimal machining parameters (350 m/min cutting speed, 3 mm radial depth of cut, and 0.32 mm/tooth feed rate) resulted in a 44.72% reduction in cutting force, 80.43% reduction in vibration amplitude, 20.41% reduction in power consumption, and 71.80% improvement in surface roughness compared to the baseline condition. Furthermore, the predictive accuracy of the optimized responses was experimentally validated with 99.603% consistency. Beyond optimization, time–frequency analysis of vibration signals (PSD and STFT) revealed that variations in mid-frequency vibration components directly influenced surface pattern formation, linking machining stability to surface integrity. Moreover, correlation analysis demonstrated strong interdependencies among surface roughness, vibration, and cutting force, indicating that surface quality is predominantly governed by dynamic cutting behavior. Overall, the study presents a comprehensive framework that integrates multi-sensor feature extraction with hybrid decision-based optimization, providing both quantifiable performance enhancements and mechanistic insights into vibration-induced surface formation during milling.

Keywords Milling · Vibration analysis · Process performance · Hybrid multi-response optimization

1 Introduction

In modern manufacturing, achieving high product quality, production efficiency, and environmental sustainability simultaneously has become a central challenge. Addressing this challenge requires the precise determination and optimization of machining parameters. In particular, the optimization of cutting parameters in machining processes directly affects key performance indicators such as surface quality, tool life, and energy consumption [1]. Although optimizing energy consumption is critically important for environmental sustainability and cost-effectiveness, evaluating this criterion in isolation is insufficient [2–5]. Considering it in conjunction with other indicators, such as surface quality, cutting forces, and dimensional tolerances, ensures more balanced and practically applicable decisions [6–9]. Therefore, the integration of multi-sensor fusion systems—capable of holistically utilizing different types of data—with methods that enable the effective analysis of such data is essential [10].

Technical Editor: Lincoln Cardoso Brandao.

✉ Bayram Sercan Bayram
sercanbayram@gazi.edu.tr

Mehmet Okan Kabakçı
mokabakci@gazi.edu.tr

İbrahim Baki Şahin
ibrahim.sahin@ahievran.edu.tr

İhsan Korkut
ikorkut@gazi.edu.tr

[1] Department of Manufacturing Engineering, Gazi University, Ankara, Türkiye

[2] Department of Mechanical Engineering, Ahi Evran University, Kirşehir, Türkiye

Multi-sensor fusion refers to an approach where data obtained from different types of sensors—such as force, vibration, or energy consumption sensors—are combined to represent the process more reliably and comprehensively. In cases where individual sensors provide limited insight, fusion techniques reveal causal relationships among data, reduce noise, improve system state estimation, and enable the simultaneous evaluation of multiple performance indicators. Consequently, more consistent and generalizable results can be achieved in the optimization of manufacturing processes [11–14].

Various studies in the literature have investigated the optimization of machining performance criteria [15–17]. For instance, in micro-milling, the effects of cutting speed and depth of cut on tool vibration and force transmissibility have been experimentally demonstrated; results indicated that increasing these parameters enhances machining stability, thereby reducing vibration and transmitted forces [18]. Regarding surface quality and energy efficiency, it has been shown that higher cutting speeds and larger tool nose radii improve surface finish, while higher material removal rates (MRR) enhance energy efficiency [19]. Furthermore, models developed for predicting energy consumption have indicated that appropriate parameter selection can lead to significant energy savings of up to 52% [20].

In another study, the effects of different cooling and lubrication conditions on surface roughness, tool wear, cutting temperature, and energy consumption were investigated to enhance the machinability of hybrid composites (Cu-6Gr/SiC-WC). It was reported that the Minimum Quantity Lubrication (MQL) environment yielded the best surface quality, while cryogenic cooling reduced tool wear, cutting temperature, and energy consumption by 67%, 31%, and 14%, respectively [21].

Similarly, Yurtkuran and Günay [22] employed Taguchi-based Grey Relational Analysis (GRA) optimization in the machining of high-alloy PH13-8Mo stainless steel, focusing on the simultaneous optimization of cutting force and surface roughness. In their study, where machining parameters such as cutting speed, feed rate, and cooling condition were optimized, the average surface roughness (Ra) values improved by 20.98% under MQL conditions and 19.86% under cryogenic cooling. Although the present discussion primarily focuses on optimization studies related to milling operations, it is worth noting that these techniques have also been widely applied across various other manufacturing processes [23–26].

Previous studies have provided significant insights into the effects of machining parameters on performance outcomes, contributing to a better understanding of process behavior. In this context, the relationships between cutting parameters and performance variables, such as surface roughness, tool wear, cutting force, or energy consumption, have generally been quantitatively evaluated using statistical methods, including Analysis of Variance (ANOVA). These analyses have offered fundamental knowledge for understanding machining mechanics and improving process stability.

Another critical aspect concerns the performance of the methods used for data analysis and optimization. Many studies in this field have proposed solutions to multi-criteria optimization problems by addressing a range of hybrid approaches. For instance, Xi et al. [27] optimized machining parameters for milling titanium alloys, considering both tool wear and energy consumption to enhance overall process efficiency. Using a hybrid algorithm known as the Radial Basis Function Neural Network–Multi-Objective Particle Swarm Optimization (RBFNN-MOPSO), they achieved a 2.65% reduction in energy consumption, a 21.44% increase in machining efficiency, and a 28.50% decrease in tool bending moment.

Similarly, Amor et al. [28] proposed a hybrid method combining GRA with the Snake Optimization algorithm to optimize the machinability of Nano TiO_2 glass fiber composites. Consequently, the Grey Relational Grade (GRG) value increased from 0.8929 to 0.9712, and the model demonstrated high accuracy with an error rate of 8.06% compared to experimental results. Nguyen et al. [29] employed integrated artificial intelligence algorithms to optimize cutting parameters during the milling of AISI 4140 steel, evaluating the NSGA-III algorithm in combination with the TOPSIS, CODAS, EDAS, and MABAC methods. The authors reported that the optimization results were consistent and reliable.

Zhang et al. [30] examined the effects of machining parameters on energy consumption, vibration, and surface quality in helical surface milling. Through a multi-objective optimization process, they achieved a 13.37% reduction in energy consumption and a 6.26% improvement in surface quality. Wu et al. [31] developed a hybrid optimization model integrating deep learning, genetic algorithm (GA), and TOPSIS techniques for the milling process, achieving a 15% improvement in both energy consumption and surface quality. Sredanovic et al. [32] analyzed the effects of depth of cut and feed per tooth on cutting force, surface roughness, burr formation, and dimensional accuracy in Inconel 718 micro-milling. Using a Taguchi–TOPSIS-based multi-objective optimization approach, they reported a channel depth deviation of 0.41 µm, burr height of 6 µm, and surface roughness of 0.24 µm.

Li et al. [33] developed a signal monitoring system to predict surface roughness during the milling of N6 nickel metal by utilizing noise, vibration, and surface texture data. Based on factor relationships determined through GRA and optimized using Particle Swarm Optimization (PSO), the Least Squares Support Vector Machine (LSSVM)-based model achieved a high reliability level with an accuracy of 92.54% and an RMS error of 0.2431 µm.

Although hybrid optimization methods integrated with artificial intelligence (AI) algorithms have demonstrated promising results in improving machining performance, several critical limitations restrict their industrial applicability. Primarily, effective and reliable training of such algorithms requires large and diverse datasets to ensure sufficient levels of generalizability and accuracy [34]. However, collecting such datasets in industrial machining environments is often costly and time-consuming. This challenge does not stem from a lack of data acquisition (DAQ) technologies but rather from the necessity of conducting numerous experimental repetitions, process interruptions, and extensive sensor calibration procedures to obtain high-quality and well-labeled data under controlled conditions [35]. These requirements significantly increase both the time and resources needed during the model development stage, thereby limiting the practical feasibility of large-scale implementations.

In contrast, statistical and multi-criteria decision-making approaches such as the Taguchi method, GRA, and the Technique for Order Preference by Similarity to Ideal Solution (TOPSIS) can deliver reliable optimization outcomes with a significantly smaller number of experiments. Thus, they represent more cost-effective and practical alternatives for industrial applications. Nevertheless, AI-based models are typically developed using datasets specific to tool–material combinations, requiring retraining and new DAQ for each new configuration. This repetitive process leads to additional resource consumption during the modeling phase.

Moreover, a considerable portion of the existing literature addresses performance indicators either individually or through limited combinations (e.g., cutting force–surface roughness or cutting force–tool wear) [36]. Such a narrow analytical focus restricts the holistic assessment of dynamic interactions occurring under real manufacturing conditions and limits the generalizability of the reported findings [37–39]. The limited data scope also hinders causal analyses of complex process interactions and prevents systematic discussions of results within the broader context of the literature [40]. Consequently, there remains a need for systematic approaches that can comprehensively evaluate the relationships between multidimensional process variables and performance outputs [41].

In this context, the primary objective of this study is to achieve a multidimensional evaluation and optimization of machining performance through the integration of a multi-sensor fusion approach with multi-criteria decision-making methods. In the proposed methodology, multiple performance indicators—including cutting forces, vibration, power consumption, and surface roughness—are holistically analyzed through sensor-based data fusion. To obtain reliable results with a minimal number of experiments, the Taguchi design of experiments was implemented. Simultaneously, the GRA method was employed to evaluate the performance criteria concurrently.

The GRA method is a statistical approach that enables the simultaneous optimization of multiple performance responses by aggregating them into a single composite performance index, known as the GRG. In this study, each performance response was first normalized using Taguchi signal-to-noise (S/N) ratios, after which the GRA method was applied to combine them into a unified performance value. This approach allowed the simultaneous assessment of multiple criteria and facilitated the holistic evaluation of overall machining performance based on a single representative metric.

To objectively determine the relative importance of the criteria, the CRITIC (Criteria Importance Through Intercriteria Correlation) weighting technique was integrated into the GRA framework. The CRITIC method is an objective weighting approach that evaluates the significance of each criterion by considering both its variability (variance) and inter-criterion correlations. By analyzing the information content and interdependencies among criteria, the CRITIC method provides a data-driven weighting scheme that does not rely on subjective expert judgments. Consequently, the relative importance of performance indicators was assessed on a consistent and mathematically rigorous basis.

The machining parameters were optimized using the obtained GRG, and the identified optimal conditions were validated through confirmation experiments. Furthermore, ANOVA was employed to statistically evaluate the effects of control factors on each performance response. Concurrently, correlation analysis was conducted to determine the interrelationships among response variables.

Additionally, the time-dependent frequency components of vibration signals were analyzed using the Short-Time Fourier Transform (STFT) method. This analysis revealed the temporal evolution of vibration behavior under different cutting conditions, and the resulting time–frequency distributions were compared with the microscopic surface texture of machined parts. In this way, the influence of vibration frequency components on surface topography was examined in detail. Moreover, PSD analysis was performed to quantitatively assess the differences in vibration energy between optimal and non-optimal machining conditions. Three-dimensional optical profilometry was used for surface roughness measurements, supported by microscopic imaging to investigate surface morphology.

This comprehensive analysis elucidates the micro-scale reflections of vibration-induced dynamic effects on surface quality through both frequency-domain (PSD/STFT) and morphological assessments, representing a distinctive contribution of this study.

In summary, this holistic methodological approach is based on the integration of multi-sensor data fusion with statistical and multi-criteria decision-making (MCDM) techniques. The study proposes a practical framework that enables the objective optimization of multiple performance criteria using a limited number of experiments, thereby contributing to the improvement of manufacturing processes in terms of energy efficiency, surface quality, and process stability. In this regard, the research aims to address the existing gap in the literature concerning data-driven, multi-criteria, and holistic analyses of machining performance.

2 Materials and methods

In this study, the edge milling of AA7075-T6 alloy was experimentally investigated to analyze the effects of different cutting parameters on multiple performance indicators, such as cutting force, vibration, power consumption, and surface roughness. The experimental trials were designed using the Taguchi L9 orthogonal array, which aims to maximize information extraction with a minimum number of experiments. Rather than directly testing factor interactions, the Taguchi method identifies optimal parameters through S/N ratio analysis to minimize process variability. Compared to full factorial designs, this method provides reliable results with fewer experimental runs and enables a systematic evaluation of machining conditions, thereby enhancing overall process performance [42]. During the experiments, force, vibration, and power consumption data were recorded using DAQ systems, and the collected signals were analyzed through signal processing and statistical methods. For the experimental study, the AA7075-T6 material was characterized using X-ray fluorescence (XRF) and hardness testing, and the results are presented in Table 1.

2.1 Experimental setup

Milling experiments were conducted using a HAAS VF-2SS 5-axis CNC machine. A 10 mm diameter, two-flute tungsten carbide end mill with a 30° helix angle was employed to machine the AA7075-T6 aluminum alloy workpiece (Fig. 1a). Cutting forces were measured at a sampling frequency of 5 kHz using a Kistler 9123 C rotary dynamometer mounted on the spindle (Fig. 1b). Vibration signals were acquired at a 100 kHz sampling rate using a YMC162A50–IEPE accelerometer attached to the workpiece (Fig. 1b) and connected to a YMC9004 DAQ system (Fig. 1c). During the cutting process, power consumption was monitored in real-time via sensors integrated into the CNC machine. The peak power consumption (kW) for each experiment was recorded (Fig. 1c and d). Surface roughness measurements were performed using a Profilm 3D optical profilometer to analyze the surface topography. A schematic illustration of the experimental setup is presented in Fig. 1.

2.2 Data collection and analysis procedure

Multi-sensor fusion (or sensor data fusion) involves combining data from multiple heterogeneous sensors to generate information that is more accurate, reliable, and comprehensive than what is obtainable from a single source. The primary objective of this approach is to overcome the limited perspective of individual measurements and to interpret complex physical phenomena from a multidimensional standpoint.

In the context of this study, multi-sensor fusion involves integrating heterogeneous data—specifically, cutting force, vibration, power consumption, and surface roughness—at both the feature and response levels to facilitate a comprehensive evaluation of machining performance. Specifically, signals were processed using appropriate analysis techniques to extract the following features for evaluation: average cutting force, average power consumption, vibration PSD values, and surface roughness (Sa) obtained via optical profilometry. These extracted features were then normalized, combined, and analyzed through a unified multi-criteria optimization framework (Taguchi–GRA–CRITIC). Consequently, rather than performing low-level signal fusion, the proposed approach implements a feature-level and decision-level fusion strategy, correlating multiple sensor-based performance indicators within a single optimization framework to achieve an integrated assessment of the machining process.

The weighting factors for each response were determined using the CRITIC method, which objectively evaluates the importance of each criterion by considering both the standard deviation (contrast intensity) and the correlation between response variables [43]. This ensures that highly informative and independent criteria receive higher weights during the GRA computation.

The multi-response optimization process was executed in several sequential stages: determination of experimental

Table 1 The chemical composition and hardness values of AA7075-T6

Element	% Al	% Zn	% Cu	% Cr	% Ti	% Fe	% Mn	% Zr	% Ni	% other
	92.432	5.481	1.534	0.169	0.144	0.112	0.037	0.035	0.016	0.04

Hardness: 177 Brinell

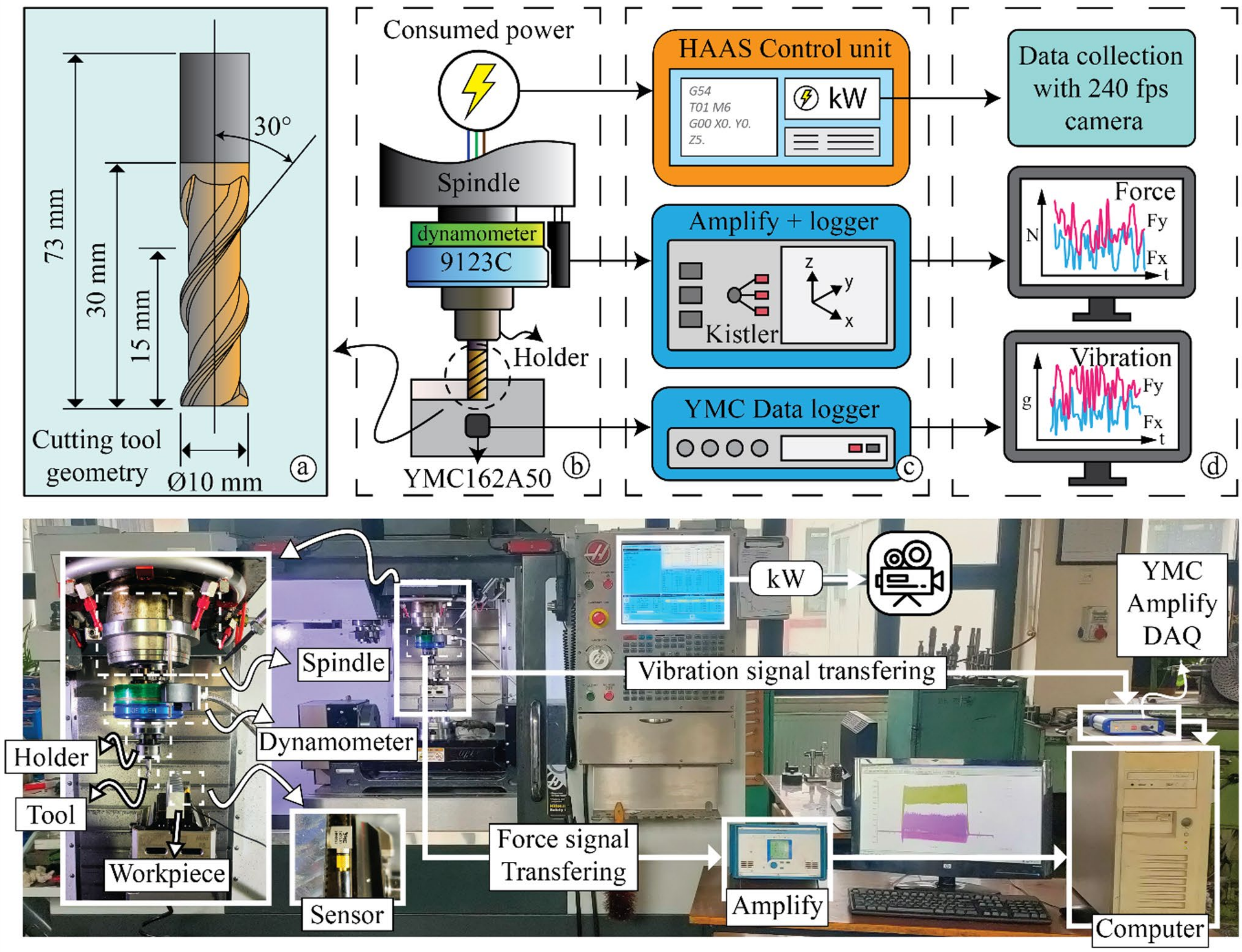

Fig. 1 Schematic and real view of the experimental setup. **a** Cutting tool geometry, **b** schematic representation of the experimental setup, **c** signal acquisition and data logging system, **d** data collection and visualization

parameters and data collection, calculation of S/N ratios, determination of Grey Relational Coefficients (GRC) and CRITIC weights, computation of the GRG, identification of optimal parameters through ANOVA, and final validation of the optimal parameter combination. The procedural steps followed in this multi-response optimization approach are illustrated in Fig. 2.

The effects of control factors on each response variable were evaluated based on S/N ratios. The cutting forces measured by the dynamometer were analyzed using the resultant force (F_n), which was calculated based on the tangential (F_t) and radial (F_r) force components. This approach enabled a comprehensive evaluation of the total force acting on the material during the cutting process. The representation and numerical values of the forces acting on the tool during machining are illustrated in Fig. 3.

The STFT method was employed to analyze the vibration frequencies occurring during the cutting process in the time domain. By dividing the signal into short time intervals and applying the Fourier transform to each window, this method enabled a detailed examination of time-varying frequency components. The PSD of the vibration signals was selected as a response variable to evaluate the effects of vibration, and the vibration energy for each experiment was calculated using the STFT method. Surface roughness was assessed using the arithmetic mean height (Sa) values obtained via optical profilometry. As the Sa parameter captures the three-dimensional texture of the surface, it allows for a comprehensive evaluation of surface quality. Finally, power consumption was continuously monitored during the cutting process via sensors integrated into the CNC machine, and the peak power consumption (kW) was recorded for each experiment. This approach enabled the identification of the effects of cutting parameters on power usage and supported the optimization of process efficiency.

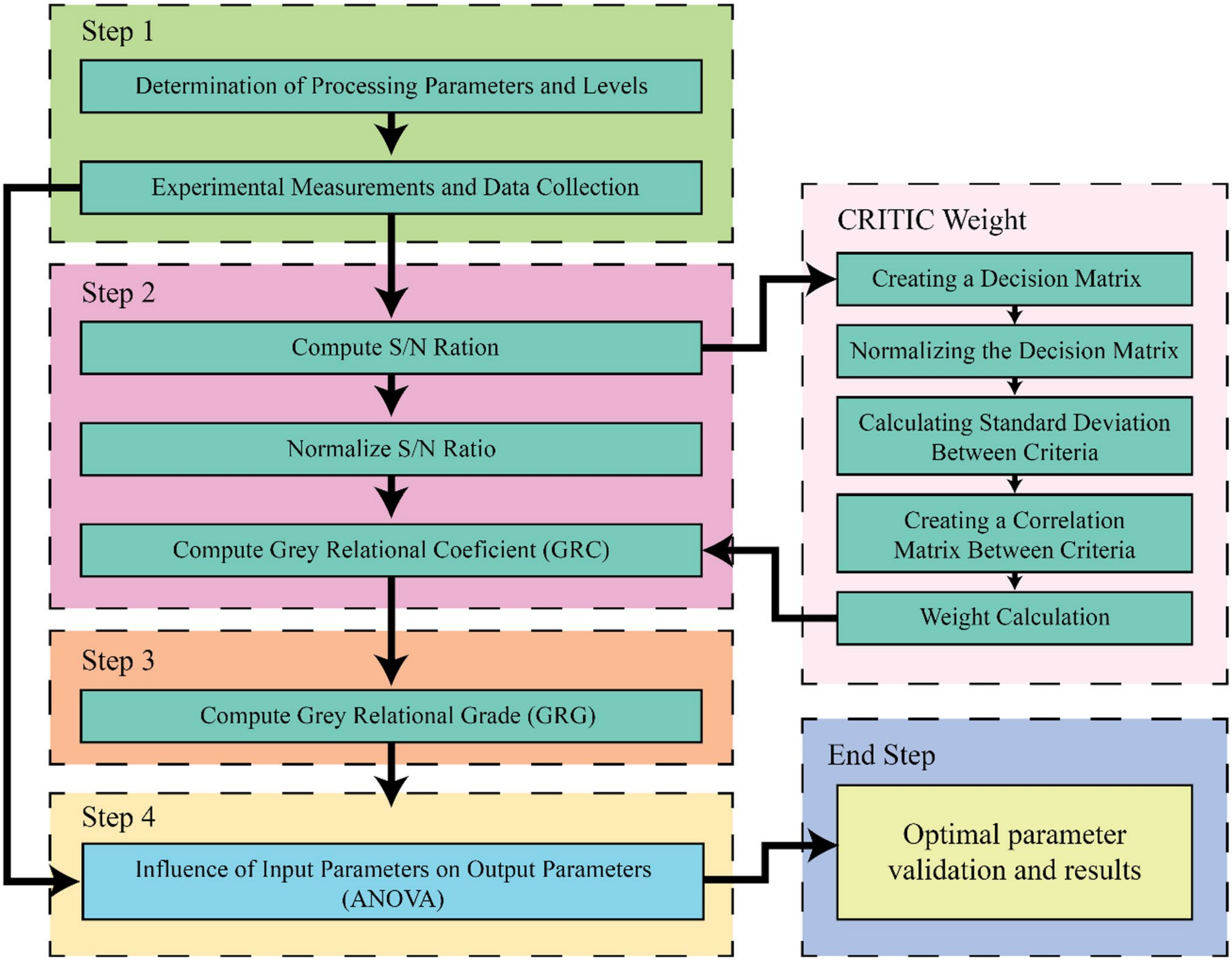

Fig. 2 Process steps of multi-response optimization

2.3 Experimental design

Experiments were conducted according to the L9 orthogonal array, with each trial repeated three times to enhance measurement reliability, minimize systematic errors, and establish a robust dataset for statistical analysis. This approach enabled a comprehensive evaluation of the effects of cutting parameters on the machining process, facilitating the determination of optimal operating conditions. The control factors and their corresponding levels employed in this study are presented in Table 2.

2.4 Hybrid Taguchi-GRA-CRITIC method based on signal-to-noise ratio

In this study, a hybrid approach combining GRA [44] based on Taguchi S/N ratios and the CRITIC method was employed to optimize machining parameters with respect to multiple response variables.

Step 1: The S/N ratios are calculated based on the desired quality characteristic. When the goal is to maximize the response, the Larger-the-Better (LTB) characteristic is applied; conversely, when minimization is desired, the Smaller-the-Better (STB) characteristic is used. In cases where the response values aim to target a specific value, the Nominal-the-Best (NTB) characteristic is employed, which considers the mean (μ) and standard deviation (σ) of the measurements. The formulations for STB, LTB, and NTB cases are provided in Eqs. 1, 2, and 3, respectively.

$$SNR_{ij} = -10log_{10}\left(\frac{1}{n_s}\sum_{r=1}^{n_s} y_{ijr}^2\right) \tag{1}$$

$$SNR_{ij} = -10log_{10}\left(\frac{1}{n_s}\sum_{r=1}^{n_s} \frac{1}{y_{ijr}^2}\right) \tag{2}$$

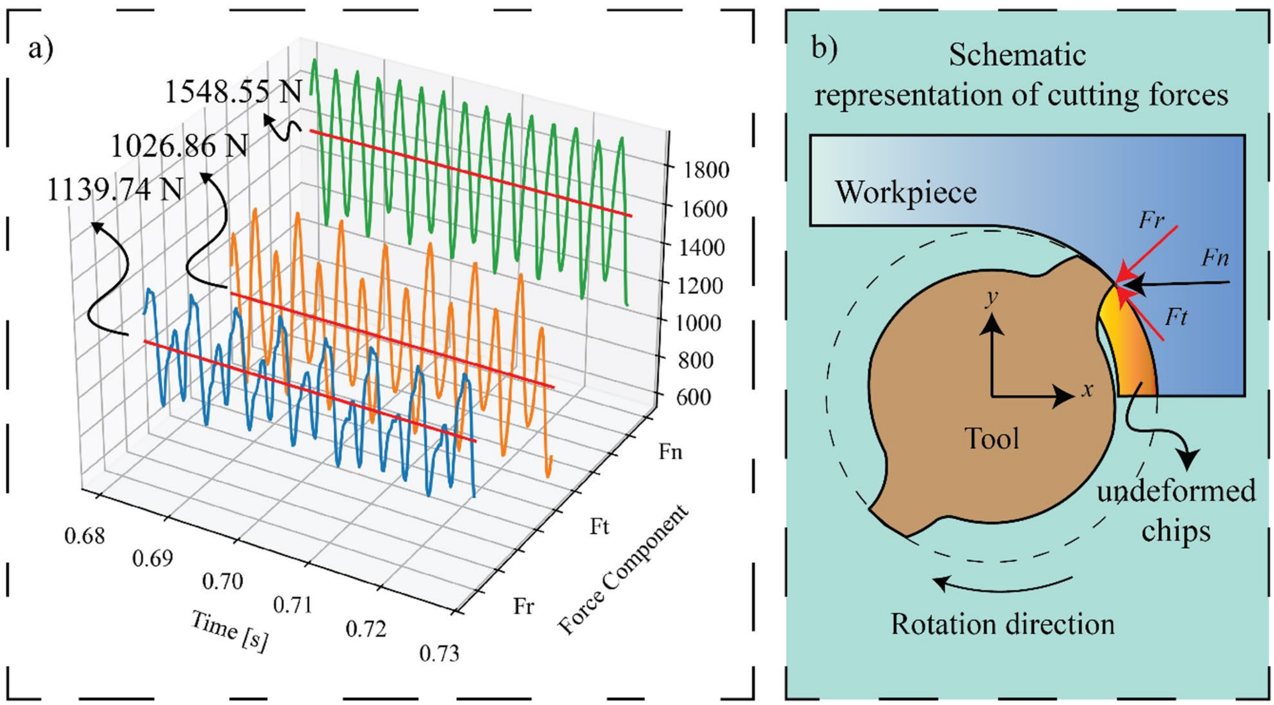

Fig. 3 Forces generated during cutting: **a** time-domain representation of the cutting force components (F_r, F_t, F_n), **b** schematic representation of cutting forces acting on the tool and workpiece

Table 2 Experimental test factors and levels

Factors	Symbol	Level 1	Level 2	Level 3
Cutting speed, V_c (m/min)	A	300	350	400
Radial depth, a_e (mm)	B	1	2	3
Feed rate, f_z (mm/tooth)	C	0.27	0.295	0.32

$$SNR_{ij} = 10log_{10}\left(\frac{\mu_{ij}^2}{\sigma_{ij}^2}\right) \tag{3}$$

where n_s is the number of repetitions, μ_{ij} is the mean, and σ_{ij} is the standard deviation.

Step 2: The calculated S/N ratios are normalized using the equations provided in Eqs. 4 and 5, depending on the type of quality characteristic.

S/N ratio for Larger-the-Better quality characteristics:

$$x_{ij} = \frac{SNR_{ij} - min_i SNR_{ij}}{max_i SNR_{ij} - min_i SNR_{ij}} \tag{4}$$

S/N ratio for Smaller-the-Better quality characteristics:

$$x_{ij} = \frac{max_i SNR_{ij} - SNR_{ij}}{max_i SNR_{ij} - min_i SNR_{ij}} \tag{5}$$

Result: $X = [x_{ij}]$ (All responses are aligned in the same direction and within the range [0,1])

Step 3: A decision matrix composed of alternatives (A_i) and criteria (C_i) is constructed, as shown in Eq. 6. Each element of the matrix (x_{ij}) represents the value of the i^{th} alternative with respect to the j^{th} criterion.

$$X = [x'_{ij}]_{mxn} = \begin{bmatrix} x'_{11} & x'_{12} & \cdots & x'_{1n} \\ x'_{21} & x'_{22} & \cdots & x'_{2n} \\ \vdots & \vdots & \ddots & \vdots \\ x'_{m1} & x'_{m2} & \cdots & x'_{mn} \end{bmatrix} \tag{6}$$

where m represents the number of alternatives, and n denotes the number of criteria.

Step 4: Following normalization via Eq. 7, the variance of each criterion (σ_j), representing the degree of variability and the information content within that criterion, is calculated using Eq. 8 for the normalized decision matrix.

$$\overline{x'_{ij}} = \frac{x'_{ij} - x'_{j\ (worst)}}{x'_{j\ (best)} - x'_{j\ (worst)}} \tag{7}$$

$$\sigma_j = \sqrt{\frac{1}{m}\sum_{i=1}^{m}\left(x'_{ij} - \overline{x'_j}\right)^2} \tag{8}$$

Step 5: The interdependence among the criteria is determined using the correlation matrix provided in Eq. 9.

$$r_{jk} = \frac{\sum_{i=1}^{m}\left(x'_{ij} - \overline{x'_j}\right)\left(x'_{ik} - \overline{x'_k}\right)}{\sum_{i=1}^{m}\left(x'_{ij} - \overline{x'_j}\right)^2 \sum_{i=1}^{m}\left(x'_{ij} - \overline{x'_j}\right)^2} \quad (9)$$

where r_{jk} is the correlation coefficient between criteria j and k.

Step 6: The calculation of the contrast measure (C_j), which accounts for both the standard deviation and the independence of each criterion, is calculated as shown in Eq. 10.

$$C_j = \sigma_j \sum_{k=1}^{n} (1 - |r_{jk}|) \quad (10)$$

Step 7: The CRITIC weights for each quality criterion are computed using Eq. 11.

$$\omega_j = \frac{C_j}{\sum_{k=1}^{n} C_k} \quad (11)$$

where ω_j is the CRITIC weight of the j-th criterion.

Step 8: The GRC for the normalized S/N ratios are calculated using Eq. 12:

$$\gamma(x_{oj}, x_{ij}) = \frac{\Delta_{min} + \xi\Delta_{max}}{\Delta_{ij} + \xi\Delta_{max}}, \ (i = 1, 2, \ldots, m; \ j = 1, 2, \ldots, n) \quad (12)$$

In this context, i represents the experiment number and j denotes the response number corresponding to that experiment. Δ_{min} and Δ_{max} are defined as shown in Eq. 13:

$$\Delta_{min} = \min_{\forall j \in i} \min_{\forall k} x_{oj} - x_{ij}, \quad \Delta_{max} = \max_{\forall j \in i} \max_{\forall k} x_{oj} - x_{ij} \quad (13)$$

- $\gamma(y_{oj}, y_{ij})$ is the GRC between x_{ij} and x_{0j}.
- A distinguishing coefficient of $\xi = 0.5$ is used.

Step 9: The GRG values are calculated using Eq. 14.

$$GRG_i = \sum_{j=1}^{n} \omega_j \cdot \gamma(y_{oj}, y_{ij}) \ , \ (i = 1, 2, \ldots, m) \quad (14)$$

Step 10: The GRG values are analyzed to determine the optimal levels. A higher GRG value indicates better output quality. Through this method, the optimal levels of the controllable factors can be identified using the Following Eqs. 15 and 16.

$$E_i = max(AGV_{ij}) - min(AGV_{ij}) \quad (15)$$

$$q^* = max_j (AGV_{ij}) \quad (16)$$

Step 11: The effects of control variables on the response outputs are determined using ANOVA. ANOVA is a statistical technique used to evaluate whether the differences between group means are statistically significant [45]. In multi-response systems, ANOVA is applied to determine the influence of various control factors on the measured response variables. This analysis identifies significant factors by evaluating the individual and interactive effects of control variables. The results are interpreted based on p-values, which indicate the statistical significance of each factor, and F-values, which represent the proportion of total variation explained by each factor.

Step 12: Finally, the predicted optimal values are experimentally validated.

3 Results and discussion

In this study, the effects of machining parameters—cutting speed (V_c, m/min), feed rate (f_z, mm/tooth), and radial depth of cut (a_e, mm)—on machining performance were analyzed through experiments designed using the Taguchi L9 (3^3) orthogonal array. The experimental results were statistically evaluated based on S/N ratios, and a hybrid Taguchi–CRITIC–GRA approach was employed for multi-response optimization. Specifically, the influence of control factors on cutting force, vibration, power consumption, and surface roughness was systematically investigated.

3.1 Evaluation of response values and control factor levels

The experimental results and their corresponding S/N ratios, derived from the Taguchi L9 orthogonal array, are summarized in Table 3. Four primary performance indicators—cutting force, vibration (PSD), power consumption, and surface roughness (Sa)—were analyzed to evaluate the influence of machining parameters on overall process behavior.

Given that the objective was to minimize these responses to enhance machining performance, each response variable was transformed into an S/N ratio based on the Smaller-the-Better (STB) criterion. Subsequently, these S/N ratios were utilized to identify the optimal levels of the control factors. The main effects plot, illustrating the mean S/N ratios for each factor level, is presented in Fig. 4.

3.1.1 Optimal parameters for cutting force (A2B3C3)

High cutting speeds generally increase temperatures in the cutting zone, potentially accelerating tool wear [46–48].

Table 3 Experimental design, the responses and S/N ratio

Runs	Factors			Responses				S/*N* ratio			
	A	B	C	Force	PSD	kW	Sa	Force	PSD	kW	Sa
1	1	1	1	1307.5	0.0516	4.9	2.773	-62.329	25.747	-13.804	-8.859
2	1	2	2	961.5	0.0226	5.2	1.571	-59.659	32.918	-14.320	-3.924
3	1	3	3	769.61	0.0091	4.5	0.810	-57.725	40.819	-13.064	1.829
4	2	1	2	983.99	0.0417	4.4	1.727	-59.860	27.597	-12.869	-4.746
5	2	2	3	681.72	0.0138	3.6	1.082	-56.672	37.202	-11.126	-0.685
6	2	3	1	1104.84	0.0417	5.2	2.196	-60.866	27.597	-14.320	-6.833
7	3	1	3	915.92	0.0202	3.8	1.036	-59.237	33.893	-11.596	-0.307
8	3	2	1	1548.55	0.0535	5.2	2.972	-63.799	25.433	-14.320	-9.461
9	3	3	2	938.92	0.0359	4.2	1.902	-59.453	28.898	-12.465	-5.584

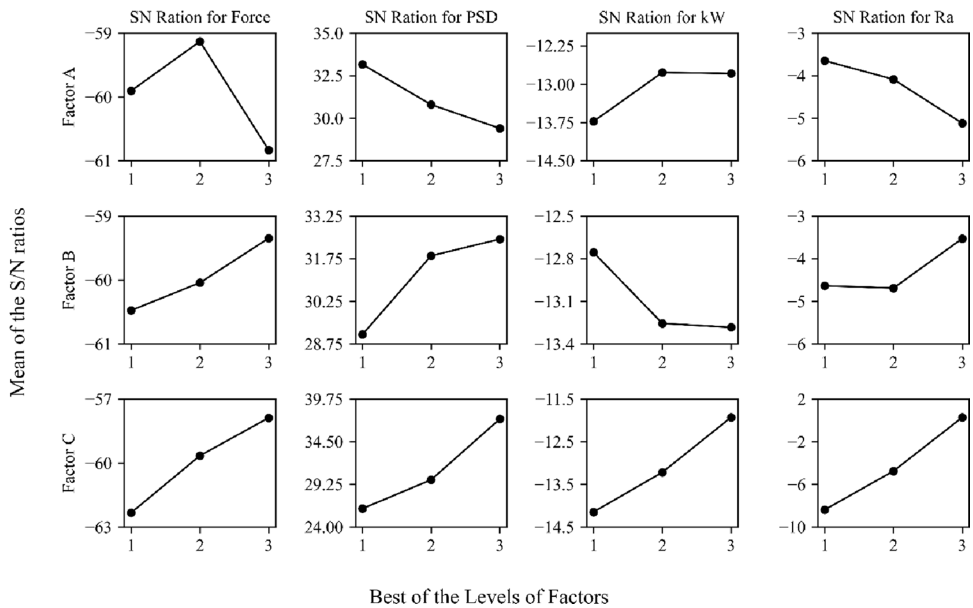

Fig. 4 Best levels of the control factors by S/N ratios

However, for aluminum alloys such as AA7075-T6, which possess high thermal conductivity, a significant portion of the generated heat is dissipated through chip evacuation, thereby mitigating this effect. Moreover, elevated temperatures in the cutting zone may reduce friction between the material and the tool, helping to control adhesion tendencies. In contrast, material deformation becomes more difficult at low cutting speeds, which can lead to increased cutting forces. In this context, moderate cutting speeds offer a more balanced performance in terms of both tool life and machining stability. Similar findings in the literature indicate that intermediate cutting speeds effectively reduce cutting forces and facilitate optimal machining conditions [49, 50].

Although an increase in feed rate is typically expected to raise cutting forces due to larger chip volume [51], a counter-phenomenon was considered in this context. At higher feed rates, the uncut chip thickness in helical cutting tools decreases, and the chip load carried by each tooth is reduced. This phenomenon is considered a significant mechanism contributing to the reduction of cutting forces [52–54]. According to the ANOVA results in Table 11, the feed rate (C) exhibits the most significant influence on the S/N ratios of the cutting force.

While the influence of radial depth of cut on cutting forces is well-documented in the literature [55, 56], the ANOVA results in Table 11 indicated no statistically significant effect in this study. This outcome may be attributed to the selection of closely spaced radial depth levels or the dominance of other parameters. Future studies employing a wider range of depth levels may elucidate this effect more clearly.

Consequently, based on the S/N ratio analysis, the optimal parameter combination for minimizing cutting force was identified as A2B3C3. This corresponds to a cutting speed of 350 m/min, a radial depth of cut of 3 mm, and a feed rate of 0.32 mm/tooth.

3.1.2 Optimal parameters for vibration performance (A1B3C3)

Based on the experimental analyses, lower cutting speed (A) levels are recommended to achieve reduced vibration amplitudes. As the cutting speed increases, the intermittent loads generated during the cutting process become more pronounced, leading to greater fluctuations in cutting load. Furthermore, high-frequency spindle rotation can trigger structural resonance in the machine tool, thereby amplifying vibrations unrelated to the cutting mechanism itself. Consequently, the combination of these effects elevates vibration levels at higher speeds [54]. Therefore, reducing the cutting speed results in lower vibration amplitudes, a finding that is consistent with the results of the present study.

According to the ANOVA results presented in Table 12, the feed rate (C) has a statistically significant effect on vibration. To minimize vibration, the Taguchi analysis (Fig. 4) indicates that the highest level of feed rate (C) is optimal; in other words, milling vibrations decrease as the feed rate increases. This phenomenon can be attributed to the fact that while a higher feed rate expands the cutting area and increases deformation resistance, it simultaneously broadens the cutting width. This action reduces the coefficient of friction, improves chip flow, and decreases dynamic cutting forces [57]. Collectively, these mechanisms contribute to the damping of vibrations.

Regarding the depth of cut, conflicting trends exist in the literature. Some studies report that increasing the depth of cut tends to elevate vibration levels due to higher cutting forces [54, 57]. However, other research suggests that vibration amplitudes may decrease at higher axial and radial depths. This perspective posits that when machining materials, localized heat generation in the cutting zone—particularly in cases where heat is not immediately dissipated—causes thermal softening of the workpiece surface. This softening reduces cutting resistance. Consequently, at higher axial or radial depths, the tool penetrates the material more easily. Furthermore, the increased engagement between the tool and the workpiece surface enhances process damping, leading to greater stability and lower vibration amplitudes.

Conversely, at lower depths of cut, the cutting tool interacts with the workpiece surface primarily through the tool edge radius rather than the cutting face. This leads to a “ploughing” or rubbing effect, which promotes vibration generation [18, 58]. The findings of the present study support this latter mechanism. In the context of aluminum alloys, material softening induced by cutting zone temperatures produces a damping effect that further reduces vibrations at increased depths. Therefore, these combined mechanisms explain the observed reduction in vibration at higher radial depths.

Consequently, the Taguchi analysis conducted in this study (Fig. 4) identified the optimal parameter combination for minimizing vibration levels as A1B3C3, corresponding to a low cutting speed (A), high radial depth of cut (B), and high feed rate (C).

3.1.3 Optimal parameters for power consumption (A2B1C3)

According to the ANOVA results presented in Table 13, the feed rate (C) accounted for the highest contribution (64.37%) to the variance in power consumption. However, the associated p-value for factor C was 0.195, indicating that it was not statistically significant ($p > 0.05$). The contributions of cutting speed (A) and radial depth of cut (B) were 15.49% and 4.56%, respectively; both factors exhibited minimal effects and failed to reach statistical significance ($p > 0.05$). Although the model’s total explanatory power appeared high ($R^2 = 84.41\%$), the relatively low adjusted coefficient of determination (Adj. $R^2 = 37.66\%$) suggested potential overfitting. This discrepancy implies that the selected factors in the reduced array did not meaningfully explain the process variability. Furthermore, the error term accounted for 15.59% of the variance, highlighting considerable unexplained variability. These findings suggested that the potential effect of the feed rate (C) required reassessment with a larger sample size. Consequently, to more accurately determine the parameters influencing power consumption, the experimental matrix was expanded to a full factorial design, and a new ANOVA was performed on the updated dataset (see Table 14 in Appendix A).

The ANOVA results derived from the full factorial design are presented in Table 15. According to these findings, the feed rate (C) was identified as the most influential parameter on power consumption, explaining 55.99% of the total variance. The associated p-value (0.000005) indicates a highly significant effect ($p < 0.01$). Additionally, cutting speed (A) contributed 18.13% to the variance and was also found to be statistically significant, with a p-value of 0.003060. In contrast, the radial depth of cut (B) accounted for only 2.76% of the variance and was not statistically significant ($p = 0.323552$). The validity of the model is supported by an R^2 value of 76.88% and an adjusted R^2 of 69.95%, demonstrating that the model robustly explains power consumption behavior. In this context, it can be concluded that feed rate and cutting speed should be prioritized in optimization studies regarding power consumption, whereas the effect of radial depth of cut appears to be negligible.

The results demonstrated that a moderate cutting speed combined with a high feed rate effectively reduces power consumption. Moreover, according to the Taguchi analysis in Fig. 4, the optimal parameter combination for minimizing power consumption was identified as A2B1C3. This finding is reinforced by the fact that lower cutting forces were achieved at the same parameter levels. In other words, the reduction in cutting forces directly contributed to the decrease in power consumption, and these two findings corroborate each other. Thus, it is evident that cutting forces govern power consumption during the machining process.

3.1.4 Optimal parameters for surface roughness (A1B3C3)

According to the ANOVA results presented in Table 16, only the feed rate (C) exhibited a statistically significant effect ($p = 0.025 < 0.05$). With a contribution ratio of 92.77%, the feed rate (C) was identified as the dominant factor governing surface roughness. In contrast, the p-values for cutting speed (A) and radial depth of cut (B) were 0.457 and 0.527, respectively. As both values exceeded the 0.05 threshold, these factors were deemed statistically insignificant. The model demonstrated notably high explanatory power, with an R^2 value of 97.66% and an adjusted R^2 of 90.63%, indicating that it captures a substantial proportion of the variability in surface roughness. The analysis confirmed that feed rate is the primary determinant of surface quality, revealing that higher feed rates resulted in reduced surface roughness values.

Notably, the results in Table 12 similarly identified the feed rate (C) as the most influential parameter affecting vibration. This consistency highlights a coherent relationship between process dynamics and surface generation: the suppression of vibrations at higher feed rates directly contributes to improved surface quality. This correlation reinforces the validity of the findings presented in this study.

Consequently, based on the Taguchi analysis results shown in Fig. 4, the parameter combination A1B3C3 is recommended as the optimal setting for achieving the lowest surface roughness.

3.2 Grey relational analysis

Evaluating each response variable individually provides valuable insights into process performance; however, such an approach is insufficient for achieving comprehensive optimization based on a single unified criterion. In practice, performance variables such as cutting force, vibration, power consumption, and surface roughness may conflict with one another. For instance, a parameter combination that minimizes vibration may compromise surface quality, or conditions that reduce power consumption may lead to increased cutting forces. Therefore, a multi-response optimization approach is required to determine the optimal machining conditions by simultaneously considering all response variables. In this context, a hybrid GRA–CRITIC method was employed to integrate all performance criteria into a single optimal performance index, allowing for the identification of the best overall combination of cutting parameters. This method enabled a holistic evaluation that considers the relative importance of each response variable. The weighted GRG coefficients, obtained by accounting for the significance of each response, are presented in Table 4.

The highest average Grade value for each factor indicates the optimal level for that factor. The difference between the maximum and minimum values (max-min) serves as an indicator of the magnitude of each factor's effect on system performance. With a delta value of 6.537, Factor C exhibited the highest impact, identifying it as the defining variable in process optimization. The fact that the A2B3C3 combination yielded the highest average values statistically confirms these levels as the optimal parameter settings. The average GRG values for Factors A, B, and C at different levels are listed in Table 17, while Fig. 5 presents the main effects plot for easier evaluation.

The ANOVA results allow for the statistical evaluation of the factors' effects on Grade values. Factor C contributed most significantly (91.93%) to the total variance, and its effect was found to be statistically significant ($p = 0.043 < 0.05$). Conversely, Factors A and B contributed

Table 4 GRA-CRITIC analysis results

Runs	Deviation sequence				CRITIC-GRC coefficient				GRA grade		Rank
	Force	PSD	kW	Sa	Force	PSD	kW	Sa	GRG	S/*N*	
1	0.794	0.980	0.838	0.947	0.055	0.080	0.168	0.060	0.091	-20.864	8
2	0.419	0.514	1.000	0.510	0.077	0.117	0.150	0.086	0.107	-19.392	6
3	0.148	0.000	0.607	0.000	0.109	0.236	0.203	0.173	0.180	-14.874	2
4	0.447	0.859	0.546	0.582	0.075	0.087	0.215	0.080	0.114	-18.857	5
5	0.000	0.235	0.000	0.223	0.141	0.161	0.449	0.120	0.218	-13.242	1
6	0.588	0.859	1.000	0.767	0.065	0.087	0.150	0.068	0.092	-20.679	7
7	0.360	0.450	0.147	0.189	0.082	0.124	0.347	0.126	0.170	-15.401	3
8	1.000	1.000	1.000	1.000	0.047	0.079	0.150	0.058	0.083	-21.584	9
9	0.390	0.775	0.419	0.657	0.079	0.093	0.244	0.075	0.123	-18.216	4

Weight of responses: Force = 0.141210, PSD = 0.236490, kW = 0.448843 and Sa = 0.173457

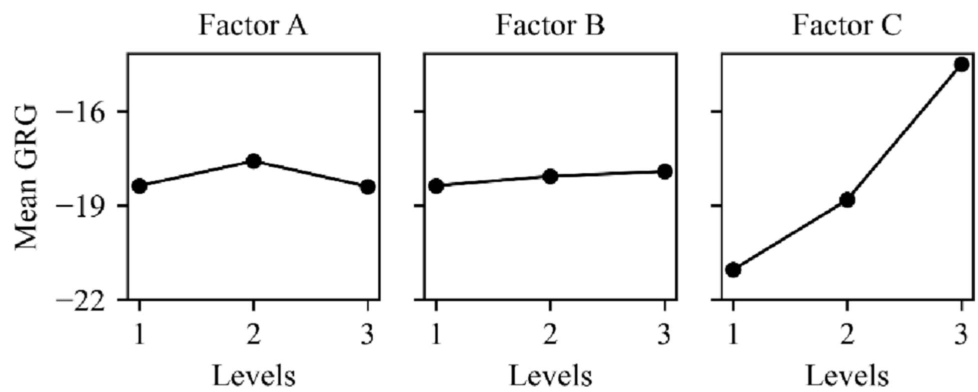

Fig. 5 Average GRG coefficients for each control factor level

Table 5 ANOVA summary table for CRITIC-GRG

Source	DF	Seq SS	Contribution	Adj SS	Adj MS	F-value	*P*-value
A	2	0.000496	2.79%	0.000496	0.000248	0.67	0.6
B	2	0.000196	1.10%	0.000196	0.000098	0.26	0.791
C	2	0.016348	91.93%	0.016348	0.008174	22	0.043
Error	2	0.000743	4.18%	0.000743	0.000372		
Total	8	0.017783	100.00%				

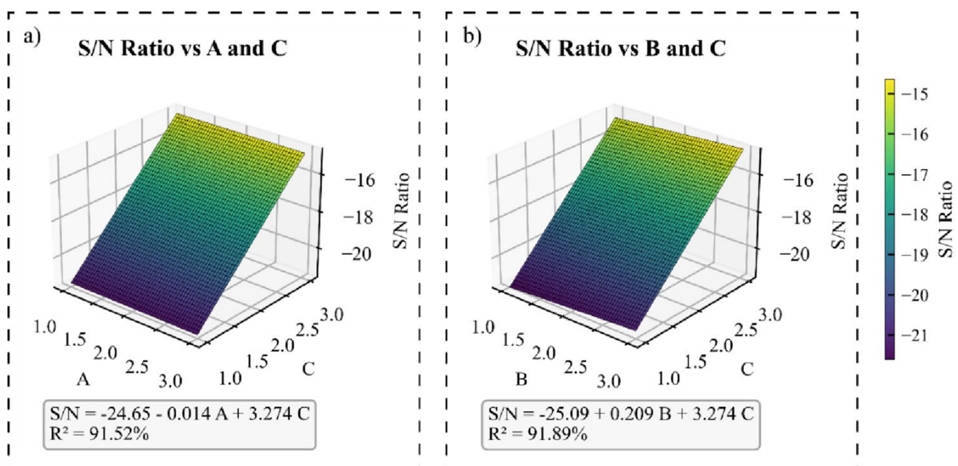

Fig. 6 3D response surface plots showing the effect of control factors on the S/N ratio: **a** S/N ratio versus cutting speed (**A**) and radial depth of cut (**B**), **b** S/N ratio versus radial depth of cut (B) and feed rate (**C**)

2.79% and 1.10%, respectively. As their p-values exceeded 0.05, the effects of these factors were deemed statistically insignificant. The error rate was calculated as 4.18%, indicating that the model possesses an acceptable level of accuracy. Consequently, it was determined that Factor C exerts a substantial effect on Grade values, while the effects of Factors A and B are negligible. The results of the ANOVA are provided in Table 5.

The evaluation of the surface plots presented in Fig. 6 is consistent with the statistical analyses performed in the previous sections. Both the Taguchi analysis and ANOVA results confirmed that Factor C has a statistically significant influence on GRA performance. In line with these findings, the surface plots demonstrate that the GRA value increases substantially with the rise of Factor C across both interaction surfaces. In contrast, Factors A and B exhibit relatively limited effects on the GRA value. Changes in Factor A do not lead to notable variations, whereas Factor B shows only a slight increasing tendency. The pronounced linear increase of GRA with respect to Factor C further reinforces that C is the most influential parameter on system performance. Moreover, the regular and linear trends observed in the surface plots indicate that the developed regression models are in good agreement with the experimental data. These consistent results across different analyses validate the critical role of Factor C in enhancing the GRA performance criterion.

3.2.1 Prediction of optimum value and validation test

A validation test was conducted to evaluate the performance of the optimal control parameters determined through the Taguchi–GRA–CRITIC hybrid method. While the GRG value predicted for the proposed A2B3C3 levels was 0.2008, the value measured in the experimental validation test was

Table 6 Results of the confirmation test

		Levels	F	PSD	kW	Sa	GRG
Initial controllable parameters		A1B1C1	1307.5	0.0516	4.9	2.773	0.0905
Optimal controllable parameters	Prediction	A2B3C3	603.157	0.011	3.889	0.709	0.2008
	Measured	A2B3C3	722.83	0.0101	3.9	0.782	0.2016
			Improvement in GRG				0.1111

Table 7 Comparative analysis of surface roughness measurements

Experimental condition	Cutting parameters (A, B, C)	Surface roughness Sa (µm)
Initial condition (used as the default reference parameter)	A1B1C1	2.773
Worst surface quality (corresponding to the least favorable outcome in the L9 orthogonal design)	A3B2C1	2.972
Rank 1 (the best parameter combination among all experiments in the L9 orthogonal array)	A2B2C3	1.082
Optimum parameter (parameters recommended based on the optimization results)	A2B3C3	0.782

0.2016, corresponding to a prediction accuracy of 99.6031%. By applying the optimal parameters, a 122.7624% increase in the GRG value was achieved compared to the initial parameter settings (A1B1C1; GRG: 0.0905).

These findings validate the accuracy of the proposed hybrid optimization method and confirm that the optimal parameters significantly improve the machining performance indicators, including vibration (PSD), power consumption, surface roughness (Sa), and cutting force. Table 6 compares the results of the validation test with the initial levels.

3.3 Surface topography

An examination of the surface roughness values presented in Table 7 facilitates a comparison between the surface morphologies of the A2B2C3 experiment (Fig. 7a), which exhibited the highest Grade value within the L9 experimental matrix, and the A3B2C1 experiment (Fig. 7b), which yielded the lowest Grade value. The sample machined using the A3B2C1 parameters, corresponding to the poorest surface finish, exhibited pronounced waviness and significant surface irregularities (Sa = 2.972 µm). In contrast, the experiment conducted under the optimal parameters (A2B3C3) demonstrated substantial improvement in surface smoothness, achieving the lowest surface roughness value (Fig. 7d; Sa = 0.782 µm). For the sample processed with the initial cutting parameters (A1B1C1), the Sa value was measured as 2.773 µm (Fig. 7c). Compared to the baseline conditions, the surface quality achieved under the optimal parameters represented a 71.80% improvement. These results indicate that cutting parameters directly govern surface quality and confirm that the proposed Taguchi–GRA–CRITIC optimization approach is effective in enhancing surface finish. The surface topographies of the samples machined under different cutting parameters are presented in Fig. 7.

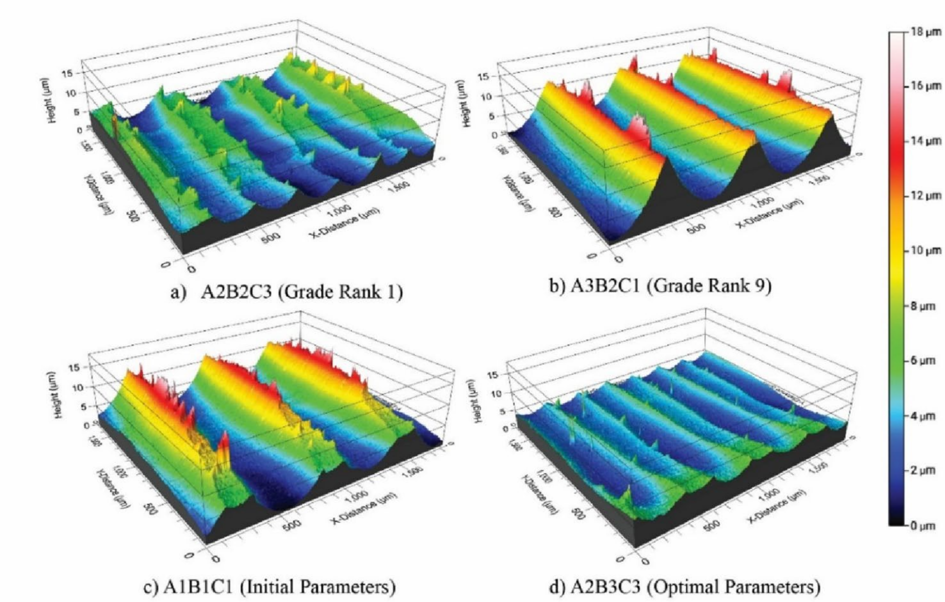

Fig. 7 3D surface topographies of machined workpieces under different parameter combinations: **a** A2B2C3 (Grade Rank 1), **b** A3B2C1 (Grade Rank 9), **c** A1B1C1 (Initial Parameters), and **d** A2B3C3 (Optimal Parameters)

3.4 Investigation of vibration frequencies and surface patterns in milling

Milling operations are susceptible to dynamic instabilities due to the complex interactions between the workpiece and the cutting tool. Among these issues, the most prevalent and detrimental is the occurrence of unstable vibrations, commonly referred to as "chatter." Chatter arises from the interaction between the natural frequencies of the tool–workpiece system and the cutting forces, negatively affecting surface quality and leading to geometric errors, reduced tolerances, and surface defects [59]. In milling processes, chatter is typically generated through a regenerative mechanism, in which the cutting edges of the tool re-engage with the wavy surface profile left by previous passes [60]. These vibrations create a self-excited loop as each tooth of the cutter engages the undulations generated by the preceding tooth [61]. This loop induces periodic variations in cutting forces; if these forces coincide with the system's natural frequencies, the resulting oscillations grow in magnitude, leading to unstable cutting conditions. Consequently, this phenomenon produces wavy surface patterns (chatter marks), increased surface roughness, and dimensional inaccuracies [62].

Flip chatter, a specific form of chatter vibration, is defined as a dynamic phenomenon characterized by period-doubling bifurcation. In this scenario, the period of vibration doubles, causing each tooth of the cutting tool to generate a distinct surface profile rather than replicating the profile created by the previous tooth. Flip chatter typically arises under specific machining regimes (e.g., specific feed rates or spindle speeds). Under these conditions, successive passes of the cutting tool leave alternating marks on the surface, resulting in widely spaced and irregular undulations, distinct dual-frequency components, and complex surface topologies [63]. The literature suggests a direct correlation between the frequency analysis of surface traces and these chatter frequencies [63, 64].

Figures 8 and 9 present the STFT graphs and machined surface geometries corresponding to the experiments conducted under the worst (A3B2C1) and optimized (A2B3C3) machining conditions, as determined by the GRA analysis. For the worst machining parameters (A3B2C1), the STFT analysis in Fig. 8e reveals that vibrations are concentrated within three distinct frequency bands throughout the process:

- High-frequency band: 38–42 kHz.
- Mid-frequency band: 15–25 kHz.
- Low-frequency band: 0.25–1 kHz.

The frequencies observed in the time–frequency domain may include structural resonances resulting from spindle and tool acceleration, as well as harmonics generated by the engagement of cutting edges with the material. Although it is difficult to conclusively identify the exact physical sources of these components based solely on visual inspection [65],

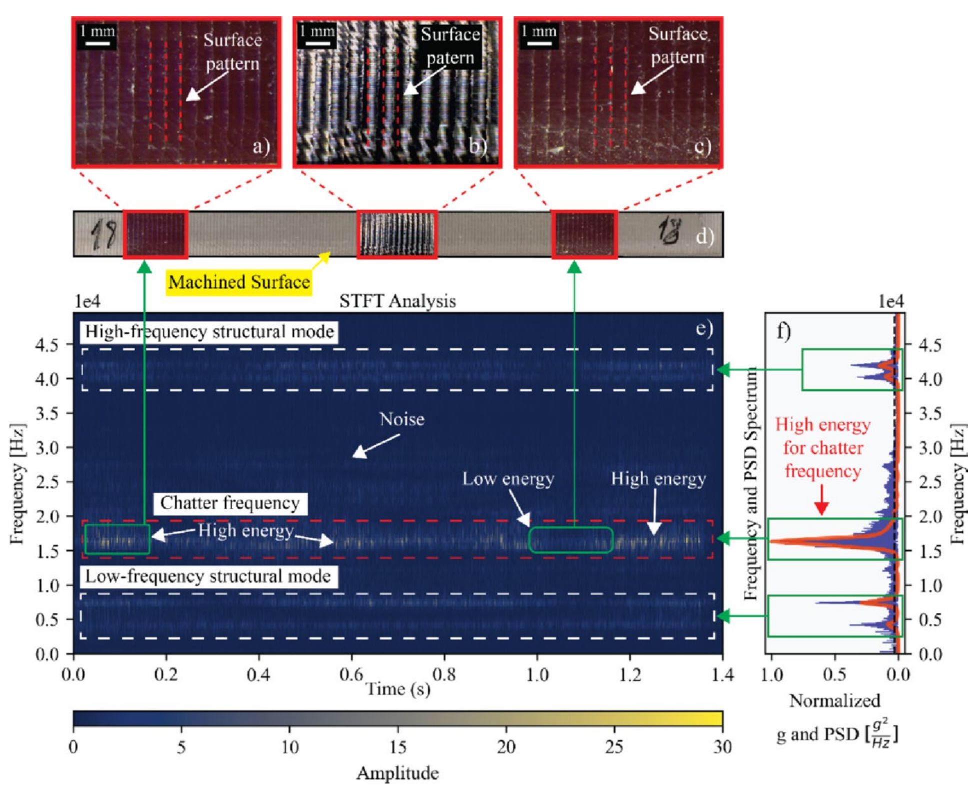

Fig. 8 Machined surface and vibration analysis (A3B2C1): **a**–**c** microscope images of surface undulations; **d** overall machined surface; **e** STFT analysis of chatter and structural frequencies; **f** PSD spectrum

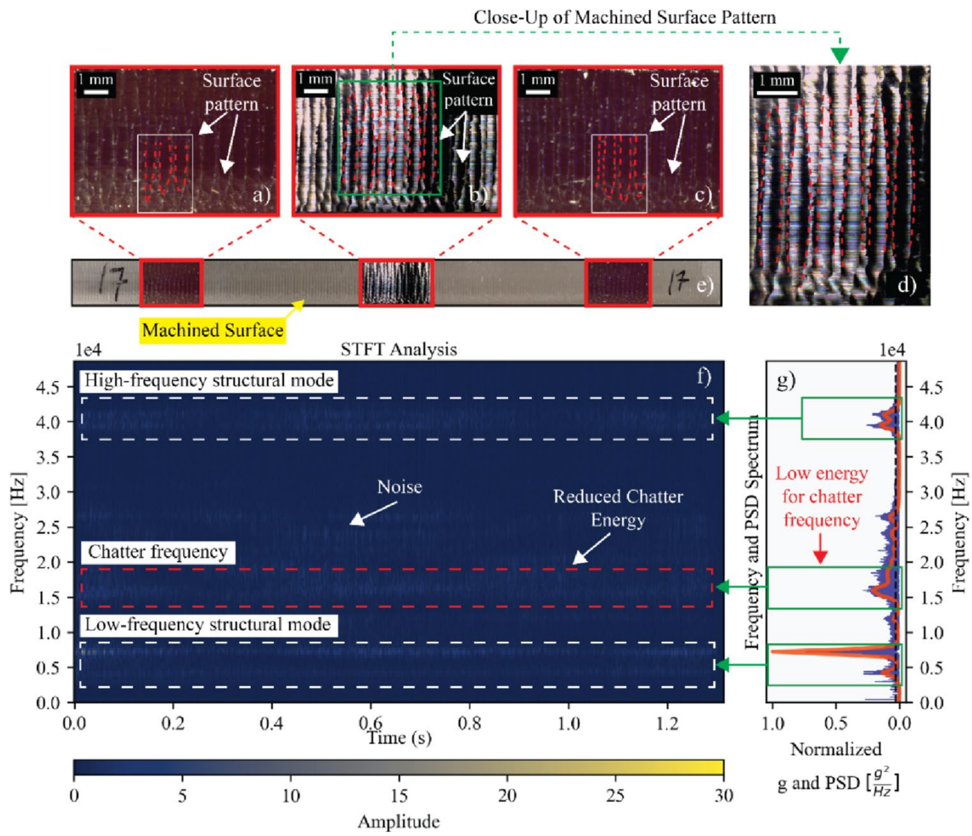

Fig. 9 Machined surface and vibration analysis (A2B3C3): **a**–**c** Microscope images of surface undulations; **d** close-up of surface pattern; **e** overall machined surface; **f** STFT analysis of chatter and structural frequencies; **g** PSD spectrum

comparing amplitude variations across experiments suggests that the fluctuations recorded—particularly within the mid-frequency range—indicate dynamic effects specific to the cutting process. Figure 8a, b, and c display microscope images of specific regions of the machined surface, while Fig. 8d shows the overall appearance of the surface. Examination of these images reveals the formation of uniform and consistent large-scale undulations. This observation corroborates the surface topography presented in Fig. 7b (obtained via optical profilometry) and suggests that chatter effects amplify the depth of these undulations.

Figure 9f presents the time–frequency analysis of the vibration signal obtained under the optimized cutting parameters (A2B3C3), which yielded the best performance metrics. When Fig. 9f is compared with Fig. 8e, a significant reduction in vibration amplitudes is observed, particularly within the mid-frequency band. This indicates that the optimized parameters effectively mitigated the dynamic loads generated during the cutting process, allowing the system to operate more stably within this frequency range. Conversely, vibration amplitudes in the low- and high-frequency regions did not change significantly compared to the worst-case scenario. Accordingly, these frequency ranges likely correspond to structural resonance frequencies, which are governed by the system's inherent dynamic characteristics rather than the cutting parameters. In conclusion, the mid-frequency range emerges as the region most sensitive to cutting parameter variations. This highlights that cutting process dynamics manifest primarily within this band, making vibration amplitudes in this region a critical indicator for assessing machining stability.

The machined surface patterns presented in Fig. 9a, b, and c reveal irregular undulations with shallow depths. This suggests that classical regenerative chatter was suppressed and surface roughness (Sa) was maintained at a low level due to the optimized parameters. However, the non-uniformity of the surface undulations indicates the persistence of low-amplitude vibration components. These irregular patterns are associated with the period-doubling phenomenon, or flip chatter. As previously described, flip chatter occurs when each tooth leaves a different cutting mark than the previous one, resulting in asymmetric and aperiodic surface undulations [63]. The optical profilometer images in Fig. 7a and d, combined with the microscope images in Fig. 9, further highlight the presence of these irregular features.

Figure 10 presents a comparative analysis of the PSD of vibration signals obtained under different cutting parameters. While the PSD curve for each experiment is plotted individually, the overall frequency–amplitude distribution is visualized using a background color-gradient heat map. This heat map statistically represents amplitude intensities across different frequency regions.

Consistent with the STFT findings, the PSD analysis highlights that the most significant amplitude variations occur in the mid-frequency bands. In contrast, no significant changes were observed in the PSD values within the low-frequency range (0.25–1 kHz). This region likely represents the structural natural frequencies of the system, which appear to be the least affected by the intermittent loads generated during cutting. Additionally, although some variations were observed in the high-frequency range (approx. 38–42 kHz) under certain conditions, the overall intensity of these changes was limited. This suggests that the influence of cutting parameters on the high-frequency range is minimal.

In summary, the PSD distribution derived from the graph is consistent with the findings of the STFT analysis. It confirms that vibration frequencies, particularly in the mid-frequency band, are highly sensitive to variations in cutting parameters.

3.4.1 Comparison of PSD characteristics under no-load, optimal, and worst cutting conditions

This section presents a comparative analysis of the PSD characteristics of vibration signals across three distinct operating states: idle (no-load), optimal cutting (A2B3C3), and worst-case cutting (A3B2C1). The objective is to elucidate how cutting conditions influence the system's dynamic response and to identify specific frequency bands that are sensitive to machining parameters. As illustrated in Fig. 11, the vibration spectra corresponding to optimal, worst-case, and idle conditions are depicted by green, blue, and red lines, respectively. The shaded regions highlight significant deviations between the worst-case and idle states, revealing pronounced peaks at 7.2 kHz, 15.9 kHz, 26.6 kHz, and 41.0 kHz. Most notably, the 15 kHz frequency band exhibited the most substantial variation, suggesting a strong correlation with dynamic cutting forces and potential machining instability. These observations provide deeper insights into the relationship between specific frequency bands and cutting parameters, corroborating the findings obtained from previous analyses.

3.5 Correlation and regression analysis

The correlation matrix presented in Fig. 12 illustrates the relationships between the numerical features extracted from the experimental trials: average cutting force, vibration (PSD), average power consumption (kW), and surface roughness (Sa). These values were organized into a structured dataset and analyzed using Pearson's correlation coefficient, which quantifies the strength and direction of linear relationships among continuous variables. The correlation matrix was computed using the corr() function in Python's Pandas library and visualized as a heatmap using Seaborn and Matplotlib. This analysis facilitated the identification of interdependencies among machining performance metrics. Significant positive correlations were observed for Force–PSD, Force–Sa, and PSD–Sa, suggesting that increases in cutting force are accompanied by higher vibration energy and rougher surface textures.

Table 8 presents the regression analysis performed for surface roughness (Sa), selected as the dependent variable. The model explains 95% of the variation in surface roughness. According to the results, the PSD variable emerges as

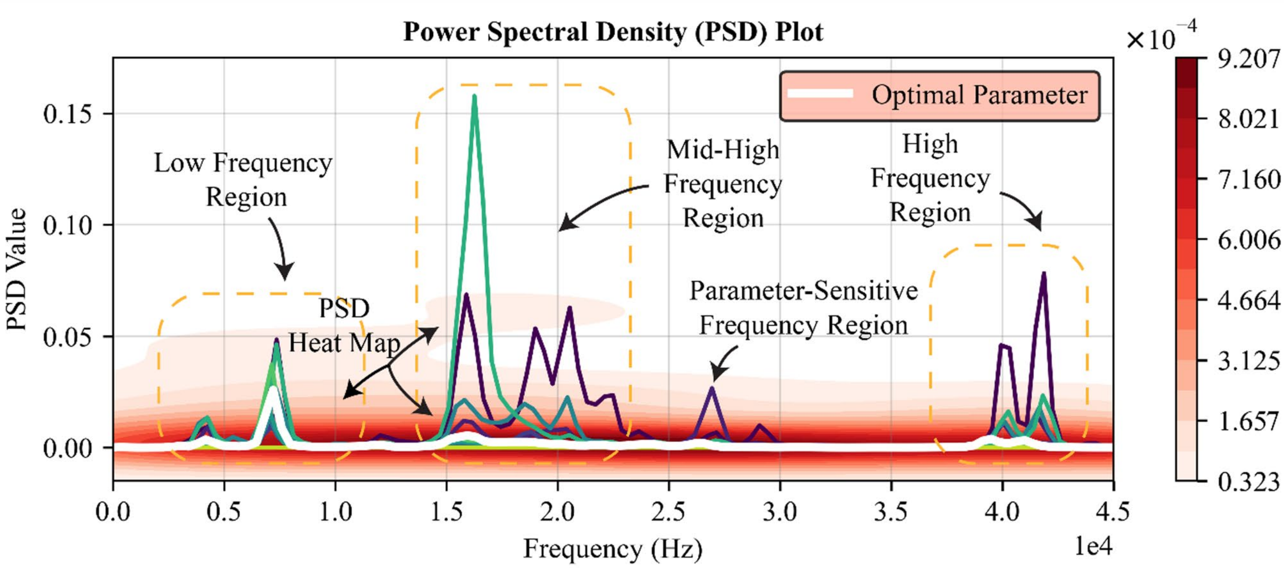

Fig. 10 Power spectrum and intensity distribution of vibration frequencies during the milling process

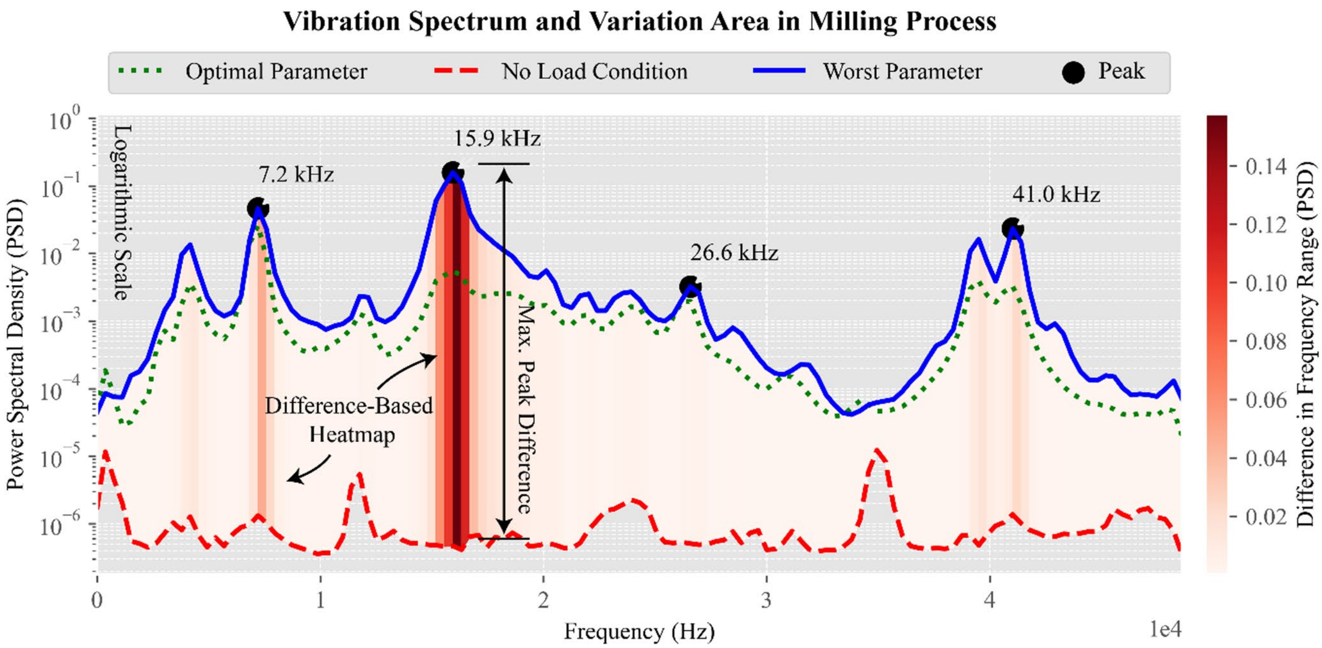

Fig. 11 Variation of vibration PSD under different machining conditions

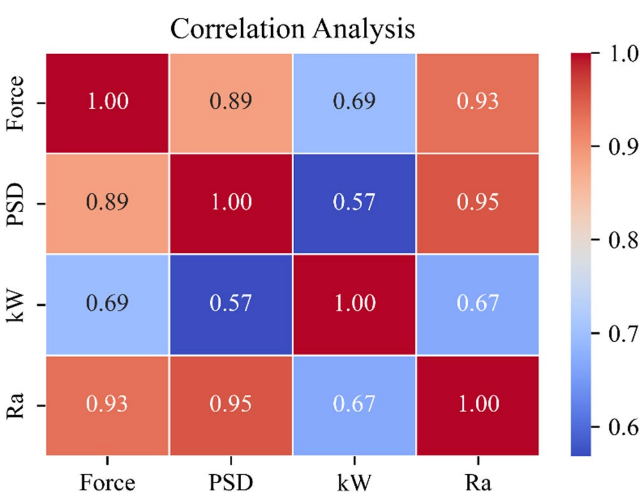

Fig. 12 Correlation matrix

Table 8 Influential factors on surface roughness

Response	Coefficient	P-value	VIF	Comment
Force	0.000914	0.250	6.15	Not statistically significant, but the correlation is strong
PSD	28.7	0.036	4.71	Statistically significant and strong effect
kW	0.119	0.520	1.97	Not statistically
Model R^2				95.07%

a statistically significant ($p = 0.036$) and influential factor on surface roughness. Conversely, despite showing high correlation values, the power consumption (kW) and cutting force variables did not exhibit statistically significant direct effects on surface roughness ($p > 0.05$).

Table 9 Variables affecting vibration

Response	Coefficient	P-value	VIF	Comment
Force	0.000058	0.011	1.93	Statistically significant and strong effect
kW	0.0024	0.745	1.93	Not statistically
Model R^2				78.77%

Table 9 presents the regression model developed for vibration (PSD), considered as the dependent variable. This model explains 78% of the variation in PSD. The analysis identifies cutting force as the most significant and strongest factor on vibration ($p = 0.011$).

In conclusion, the statistical analyses reveal a causal chain: vibration (PSD) is the primary determinant of surface roughness (Sa), while cutting force is the significant driver of vibration (PSD). According to the results, the power consumption (kW) variable does not exhibit a statistically significant effect on either PSD or Sa in the regression models. This lack of significance is likely attributed to the fact that power consumption is a cumulative output of the process rather than a direct governing factor of surface generation or dynamic stability. In a separate regression analysis conducted with power consumption as the dependent variable, the model yielded an R^2 value of 53.61%, whereas the adjusted R^2 value was only 25.78%. This substantial discrepancy indicates a potential risk of overfitting. Although the power consumption variable was not found to be statistically significant in these specific regression models, it remains a critical parameter that may influence the system through indirect effects or complex interactions not captured by linear models.

3.6 Comparison with literature

Table 10 presents a comparative analysis of the performance of the proposed Taguchi–GRA–CRITIC framework against findings from previous machining optimization studies. Research conducted by Shi et al. [66] and Esme [67], who applied the Taguchi–GRA approach, demonstrated moderate improvements in surface roughness ranging from 32% to 64%, while increases in the GRG index remained below 10–15%. In another study, Sarıkaya et al. [68] incorporated multiple response variables—such as cutting force, vibration, and surface roughness—achieving performance enhancements of 34–69% and a 42.9% increase in GRG. Utilizing the TOPSIS method, Jebaraj et al. [69] achieved a 51.40% improvement in the closeness coefficient (CC). Similarly, Sur et al. [70] reported improvements of 63.81% and 34.71% in cutting force and surface roughness, respectively, using the same technique. Suneesh and Sivapragash [71] evaluated GRA and TOPSIS as distinct approaches, reporting increases of 38.20% and 29.91% in GRG and CC, respectively, along with 8–20% improvements in cutting force and surface roughness.

In contrast, the present study achieved superior results: a 44.72% reduction in cutting force, an 80.43% reduction in vibration amplitude, a 20.41% reduction in power consumption, and a 71.80% improvement in surface roughness, accompanied by a 122.76% increase in GRG relative to the baseline parameters. While previous studies have reported comparable improvements in individual metrics, the magnitude and consistency of the performance gains across all response variables in the current study are substantially higher. It is acknowledged that direct quantitative comparisons are inherently limited due to variations in experimental conditions, tool–workpiece materials, control factors, and response variables. Nevertheless, this benchmarking provides a meaningful reference for evaluating the relative efficacy of the proposed approach. In conclusion, the hybrid Taguchi–GRA–CRITIC methodology demonstrates superior optimization capability and statistical robustness, offering a comprehensive and reliable multi-response optimization strategy suitable for real-world industrial machining applications.

4 Conclusions

In this study, the milling performance of AA7075-T6 aluminum alloy was experimentally investigated and optimized with respect to cutting force, vibration, power consumption, and surface roughness. The experimental design was structured based on a Taguchi L9 orthogonal array using three levels of cutting speed, feed rate, and radial depth of cut as control parameters. A hybrid multi-response optimization method was employed to integrate Taguchi S/N ratios, GRA, and the CRITIC weighting method. The optimal parameter combination was determined and experimentally validated, achieving a prediction accuracy of 99.603%. Furthermore, vibration behavior was evaluated using STFT and PSD analyses, and the effects of vibration on surface geometry were examined. The key findings are summarized as follows:

- The optimal machining performance was achieved with the parameter combination A2B3C3, which resulted in improvements of 44.72% in cutting force, 80.43% in vibration amplitude, 20.41% in power consumption, and 71.80% in surface roughness compared to the baseline conditions.
- Feed rate was identified as the most statistically significant parameter influencing all performance criteria ($p < 0.045$).

Table 10 Comparison of the proposed Taguchi–GRA–CRITIC optimization results with previous machining optimization studies

Study	Optimization method	Response variables	Performance improvement (%)	Improvement in optimization index (GRG or CC)
Shi et al. [66]	Taguchi–GRA	Residual stress, Hardness, Ra	Ra ↓ 32.57%	+ 15.28% for GRG
Esme [67]	Taguchi–GRA	Ra	Ra ↓ 64.28%	+ 6.94% for GRG
Sankaya et al. [68]	Taguchi–GRA	F_x, Vibration, Ra	F_x ↓ 69.07%, Vib ↓ 40.65%, Ra ↓ 34.22%	+ 42.9% for GRG
Jebaraj et al. [69]	TOPSIS	Temperature, F_x, F_y, Ra	F_x ↓ 53.95%, F_y ↓ 60.82% Ra ↓ 44.56%	+ 51.40% for CC
Sur et al. [70]	TOPSIS	F, Ra	F ↓ 63.81%, Ra ↓ 34.71%	-
Suneesh & Sivapragash [71]	GRA, TOPSIS	Tool wear, F_x, R_a	F_x ↓ 8.89%, F_y ↓ 18.06%, Ra ↓ 12.12%,	+ 38.20% for GRG + 29.9% for CC
Present study	Taguchi–GRA–CRITIC	F, Vibration, Power, Sa	F ↓ 44.72%, Vib ↓ 80.43%, Power ↓ 20.41%, Ra ↓ 71.80%	+122.76% for GRG

While previous studies typically utilized the linear profile parameter Ra, the present study employs the areal parameter Sa for a more comprehensive topographic assessment. Comparisons are based on percentage improvements

- Vibrations were found to be highly sensitive to cutting parameters, particularly within the frequency range of 15–25 kHz (chatter frequencies). The worst parameter combination (A3B2C1) resulted in regular and deep surface undulations (classical chatter marks), whereas the optimal parameters (A2B3C3) significantly reduced these chatter effects. However, irregular yet shallower surface undulations were observed, contributing to low-amplitude vibrations associated with flip chatter.
- Increasing the cutting speed increased the frequency of intermittent impact loads during the cutting process, amplifying fluctuations in cutting forces and elevating vibration levels. Additionally, high-frequency spindle motion potentially excited structural resonances in the machine tool, generating vibrations unrelated to the cutting mechanism and contributing to overall vibration levels.
- Power consumption was found to be directly correlated with cutting forces. Any parameter that increased cutting forces also increased power consumption, emphasizing the importance of cutting force optimization for enhancing energy efficiency.

The findings obtained from the proposed Taguchi–GRA–CRITIC optimization framework demonstrate that cutting speed has a statistically significant effect on reducing cutting forces, a result consistent with physical interpretations reported in the literature. However, the integrated multi-criteria evaluation enabled the quantitative identification of the optimal cutting speed level (350 m/min), which resulted in a 44.72% reduction in cutting force compared to the initial machining condition. Therefore, rather than merely confirming a known trend, the proposed optimization method precisely determines the machining parameter combination that yields the most balanced overall performance.

Similarly, although the influence of cutting parameters on vibration behavior is well established, the feature- and decision-level fusion approach utilized in this study revealed that vibration reduction is strongly linked to improvements in surface integrity, as evidenced by the correlation between PSD values and Sa parameters. The multi-response optimization method identified feed per tooth (0.32 mm/tooth) and radial depth (3 mm) as key factors in simultaneously minimizing vibration and surface roughness, providing a holistic performance enhancement rather than isolated parameter tuning.

The proposed methodology enabled the coordinated optimization of cutting force, vibration, power consumption, and surface roughness, which are typically treated independently in conventional machining studies. Therefore, the primary contribution of this work lies not in reaffirming known mechanistic interactions, but in demonstrating that the integration of the Taguchi–GRA–CRITIC method with multi-sensor feature fusion enables the determination of an optimal machining configuration that balances multiple performance criteria simultaneously, thereby supporting data-driven decision-making in manufacturing environments.

Appendix A

Experimental dataset and grey relational analysis results

Appendix A contains the raw and processed data employed in the Taguchi-based grey relational analysis, including experimental runs, normalized responses, and calculated GRA ranking results for each parameter combination.

See Tables 11, 12, 13, 14, 15, 16 and 17.

Table 11 ANOVA results for cutting force based on S/N ratios

Source	DF	Seq SS	Contribution	Adj SS	Adj MS	F-value	*P*-value
A	2	4.330	11.44%	4.330	2.165	3.015	0.249
B	2	1.941	5.13%	1.941	0.970	1.351	0.425
C	2	30.143	79.64%	30.143	15.071	20.984	0.045
Error	2	1.436	3.80%	1.436	0.718		
Total	8	37.850	100.00%				

Model summary	R-sq	R-sq(adj)
	96.20%	84.82%

Table 12 ANOVA results of PSD values according to S/N ratios

Source	DF	Seq SS	Contribution	Adj SS	Adj MS	F-value	*P*-value
A	2	21.603	9.27%	21.603	10.802	17.88	0.053
B	2	19.312	8.29%	19.312	9.656	15.98	0.059
C	2	190.835	81.92%	190.835	95.418	157.92	0.006
Error	2	1.208	0.52%	1.208	0.604		
Total	8	232.959	100.00%				
Model summary	R-sq	R-sq(adj)					
	99.48%	97.93%					

Table 13 ANOVA results of power consumption values according to S/N ratios

Source	DF	Seq SS	Contribution	Adj SS	Adj MS	F-value	*P*-value
A	2	1.7934	15.49%	1.7934	0.897	0.99	0.502
B	2	0.5276	4.56%	0.5276	0.264	0.29	0.774
C	2	7.4529	64.37%	7.4529	3.726	4.13	0.195
Error	2	1.8046	15.59%	1.8046	0.902		
Model summary	R-sq	R-sq(adj)					
	84.41%	37.66%					

Table 14 Updated experimental dataset and corresponding S/N ratios based on the full factorial design for power consumption analysis

Runs	Factors			Responses				S/*N* ratio			
	A	B	C	Force	PSD	kW	Sa	Force	PSD	kW	Sa
1	1	1	1	1307.50	0.0516	4.9	2.7730	-62.329	25.747	-13.804	-8.859
2	1	1	2	1023.26	0.0289	5.2	2.2180	-60.200	30.782	-14.320	-6.919
3	1	1	3	715.93	0.0054	4.3	1.6310	-57.097	45.352	-12.669	-4.249
4	1	2	1	1332.78	0.0478	5.1	2.4380	-62.495	26.411	-14.151	-7.741
5	1	2	2	961.50	0.0226	5.2	1.5710	-59.659	32.918	-14.320	-3.924
6	1	2	3	797.37	0.0069	4.9	0.9840	-58.033	43.223	-13.804	0.140
7	1	3	1	1213.24	0.0394	5.5	2.1850	-61.679	28.090	-14.807	-6.789
8	1	3	2	993.71	0.0265	4.9	1.5510	-59.945	31.535	-13.804	-3.812
9	1	3	3	769.61	0.0091	4.5	0.8101	-57.725	40.819	-13.064	1.829
10	2	1	1	1267.76	0.0825	6.0	2.9690	-62.061	21.671	-15.563	-9.452
11	2	1	2	983.99	0.0417	4.4	1.7270	-59.860	27.597	-12.869	-4.746
12	2	1	3	748.66	0.0211	4.3	1.2800	-57.486	33.514	-12.669	-2.144
13	2	2	1	1142.48	0.0431	5.3	1.5580	-61.157	27.310	-14.486	-3.851
14	2	2	2	1041.88	0.0324	4.9	1.4450	-60.356	29.789	-13.804	-3.197
15	2	2	3	681.72	0.0138	3.6	1.0820	-56.672	37.202	-11.126	-0.685
16	2	3	1	1104.84	0.0417	5.2	2.1960	-60.866	27.597	-14.320	-6.833
17	2	3	2	936.29	0.0274	4.8	0.9857	-59.428	31.245	-13.625	0.125
18	2	3	3	722.83	0.0101	3.9	0.7820	-57.181	39.914	-11.821	2.136
19	3	1	1	1547.56	0.0926	5.6	2.9690	-63.793	20.668	-14.964	-9.452
20	3	1	2	1345.35	0.0443	4.5	2.3510	-62.577	27.072	-13.064	-7.425
21	3	1	3	915.92	0.0202	3.8	1.0360	-59.237	33.893	-11.596	-0.307
22	3	2	1	1548.55	0.0535	5.2	2.9720	-63.799	25.433	-14.320	-9.461
23	3	2	2	1179.32	0.0310	4.3	2.4350	-61.433	30.173	-12.669	-7.730
24	3	2	3	748.94	0.0166	3.4	1.7820	-57.489	35.598	-10.630	-5.018
25	3	3	1	1271.03	0.0521	4.3	2.2500	-62.083	25.663	-12.669	-7.044
26	3	3	2	938.92	0.0359	4.2	1.9020	-59.453	28.898	-12.465	-5.584
27	3	3	3	700.72	0.0227	3.2	1.7970	-56.911	32.879	-10.103	-5.091

Table 15 ANOVA results of power consumption values according to S/N ratios for the full factorial experimental design

Source	DF	Seq SS	Contribution	Adj SS	Adj MS	F-value	*P*-value
A (Cutting speed)	2	8.563	18.13%	8.563	4.2814	7.84	0.003060
B (Feed rate)	2	1.304	2.76%	1.304	0.6522	1.19	0.323552
C (Feed rate)	2	26.447	55.99%	26.447	13.2237	24.22	0.000005
Error	20	10.920	23.12%	10.920	0.5460		
Total	26	47.235	100.00%				
Model summary		R-sq			R-sq(adj)		
		76.88%			69.95%		

Table 16 ANOVA results of surface roughness values according to S/N ratios

Source	DF	Seq SS	Contribution	Adj SS	Adj MS	F-value	*P*-value
A	2	3.401	2.78%	3.401	1.701	1.19	0.457
B	2	2.577	2.11%	2.577	1.289	0.90	0.527
C	2	113.557	92.77%	113.557	56.779	39.60	0.025
Error	2	2.868	2.34%	2.868	1.434		
Total	8	122.404	100.00%				
Model summary		R-sq	R-sq(adj)				
		97.66%	90.63%				

Table 17 Average GRG values for control factor levels

Level	Factors		
	A	B	C
1	-18.377	-18.374	-21.042
2	**-17.593**	-18.072	-18.822
3	-18.400	**-17.923**	**-14.505**
Max-min	0.808	0.451	6.537
Rank	2	3	1

The bold values indicate the maximum average GRG values, representing the optimal levels of the control factors

Acknowledgements The authors conducted this study in the Machinability Laboratory of the Manufacturing Engineering Department at Gazi University. The authors would like to thank Gazi University for the infrastructure support provided.

Funding Open access funding provided by the Scientific and Technological Research Council of Türkiye (TÜBİTAK).

Data availability The data used in this study are confidential.

Declarations

Conflict of interest The authors declare that they have no known competing financial interests or personal relationships that could have appeared to influence the work reported in this paper.

References

1. Tebassi H, Yallese MA, Belhadi S (2023) Optimization and machinability assessment at the optimal solutions across Taguchi OA, GRA, and BBD: an overall view. Arab J Sci Eng 48:12455–12483. https://doi.org/10.1007/s13369-023-07825-6
2. Feng C, Qin E, Li W et al (2024) Energy consumption and surface roughness modelling for multi-objective optimisation of machining processes. Int J Adv Manuf Technol 133:5065–5087. https://doi.org/10.1007/s00170-024-14043-3
3. Xiao Q, Li C, Tang Y et al (2019) Multi-component energy modeling and optimization for sustainable dry gear hobbing. Energy 187:115911. https://doi.org/10.1016/j.energy.2019.115911
4. Zhao GY, Liu ZY, He Y et al (2017) Energy consumption in machining: Classification, prediction, and reduction strategy. Energy 133:142–157. https://doi.org/10.1016/j.energy.2017.05.110
5. Arif Muhammad, Stroud Ian A, Akten Olcay (2014) A model to determine the optimal parameters in a machining process for the most profitable utilization of machining energy. Proc Inst Mech Eng B J Eng Manuf 229:266–274. https://doi.org/10.1177/0954405414527960
6. Nguyen V-H, Tien-Thinh L, Anh-Tu N et al (2024) Multiobjective optimization of end milling parameters for enhanced machining performance on 42CrMo4 using machine learning and NSGA-III. Mach Sci Technol 28:744–776. https://doi.org/10.1080/10910344.2024.2381191
7. Cui Z, Liu H, Wu L et al (2024) Cutting force and surface quality in ultra-precision milling of oxygen-free copper under different

cutting strategies. J Manuf Process 131:2420–2442. https://doi.org/10.1016/j.jmapro.2024.10.056
8. Feng C, Guo H, Zhang J et al (2022) A systematic method of optimization of machining parameters considering energy consumption, machining time, and surface roughness with experimental analysis. Int J Adv Manuf Technol 119:7383–7401. https://doi.org/10.1007/s00170-022-08772-6
9. Zhang X, Yu T, Dai Y et al (2020) Energy consumption considering tool wear and optimization of cutting parameters in micro milling process. Int J Mech Sci 178:105628. https://doi.org/10.1016/j.ijmecsci.2020.105628
10. Bai L, Zhang J, Budak E et al (2024) Vibration energy-based indicators for multi-target condition monitoring in milling operations. J Manuf Syst 77:284–300. https://doi.org/10.1016/j.jmsy.2024.09.015
11. Du H, Wang Q, Zhang X et al (2024) A novel multi-sensor hybrid fusion framework. Meas Sci Technol 35:086105. https://doi.org/10.1088/1361-6501/ad42c4
12. Wang Q, Yu L, Hao L et al (2025) An adaptive transfer fault detection method for rotary machine with multi-sensor information fusion. J Intell Manuf 36:4695–4710. https://doi.org/10.1007/s10845-024-02469-1
13. Zheng M, Yang W, Si Y, Zheng T (2025) Milling chatter identification based on deep convolutional neural networks and Multi-Sensor fusion. J Vib Eng Technol 13:345. https://doi.org/10.1007/s42417-025-01847-0
14. Sun L, Huang X, Jiang Z et al (2025) Multi-source heterogeneous sensor information fusion framework for intelligent online chatter detection in different milling conditions. Knowl Based Syst 330:114488. https://doi.org/10.1016/j.knosys.2025.114488
15. de Oliveira NB, Peruchi RS, Rotella Junior P, de Brito TG (2023) Modeling and optimization of steel end milling process: a review on empirical studies. J Brazilian Soc Mech Sci Eng 45:593. https://doi.org/10.1007/s40430-023-04503-4
16. Somasundaram M, Dinesh Kumar K, NarendraKumar U, Raja Annamalai A (2024) Dry milling of stir-cast and heat-treated EV31A magnesium alloy: an experimental investigation based on the multi-criteria optimization method. Measurement 231:114613. https://doi.org/10.1016/j.measurement.2024.114613
17. Bayram BS, Atila Ü, Uzun G et al (2025) A robust mechanistic–metaheuristic hybrid approach for predicting milling force coefficients. Proc Institution Mech Eng Part E: J Process Mech Eng. https://doi.org/10.1177/09544089251390127
18. Singh C, Das A, Bajpai V, Chandravanshi ML (2023) Effects of process parameters on tool vibration and force transmissibility in high-speed micro-milling machine. J Brazilian Soc Mech Sci Eng 45:343. https://doi.org/10.1007/s40430-023-04266-y
19. Nguyen T-T, Nguyen T-A, Trinh Q-H (2020) Optimization of milling parameters for energy savings and surface quality. Arab J Sci Eng 45:9111–9125. https://doi.org/10.1007/s13369-020-04679-0
20. Wang Q, Zhang D, Tang K, Zhang Y (2019) Energy consumption model for milling processes considering auxiliary load loss and its applications. Int J Adv Manuf Technol 105:4309–4323. https://doi.org/10.1007/s00170-019-04479-3
21. Usca ÜA, Şap S, Uzun M, Değirmenci Ü (2024) Assessment of the machinability and energy consumption characteristics of Cu–6Gr hybrid composites under sustainable operating. J Brazilian Soc Mech Sci Eng 46:221. https://doi.org/10.1007/s40430-024-04815-z
22. Yurtkuran H, Günay M (2024) Predictive modelling and optimization for machinability indicators in cleaner milling of PH13-8Mo using sustainable cutting environments. J Brazilian Soc Mech Sci Eng 46:319. https://doi.org/10.1007/s40430-024-04897-9
23. Ouahiba T, Hamid H, Selma B, Laouar L (2024) Multi-objective optimization of slide diamond burnishing parameters for enhanced fatigue resistance of AISI 52100 steel. J Brazilian Soc Mech Sci Eng 46:451. https://doi.org/10.1007/s40430-024-05001-x
24. Amri R, Laamouri A, Fathallah R (2023) Multiobjective optimization of waterjet peening effects on high-cycle fatigue life of Al-7075-T6 alloy. J Brazilian Soc Mech Sci Eng 46:31. https://doi.org/10.1007/s40430-023-04613-z
25. Nair A, Bizoń W, Skoczypiec S et al (2024) Experimental exploration and optimization of dual-channel electrode micro-drilling in inconel 617 using electrical discharge machining. J Brazilian Soc Mech Sci Eng 46:673. https://doi.org/10.1007/s40430-024-05247-5
26. Saeheaw T (2022) Application of integrated CRITIC and GRA-based Taguchi method for multiple quality characteristics optimization in laser-welded blanks. Heliyon 8:e11349. https://doi.org/10.1016/j.heliyon.2022.e11349
27. Xi L, Li L, Li L et al (2024) Parameter optimization of titanium alloy considering energy efficiency and tool wear based on RBFNN-MOPSO algorithm in milling. J Manuf Process 122:97–111. https://doi.org/10.1016/j.jmapro.2024.05.070
28. Amor N, Tayyab Noman M, Petru M et al (2024) Machining performance of TiO2 embedded-glass fiber reinforced composites with snake optimizer. Measurement 227:114253. https://doi.org/10.1016/j.measurement.2024.114253
29. Nguyen V-H, Le T-T, Nguyen A-T et al (2025) Optimization of milling conditions for AISI 4140 steel using an integrated machine learning-multi objective optimization-multi criteria decision making framework. Measurement 242:115837. https://doi.org/10.1016/j.measurement.2024.115837
30. Zhang W, Sun X, Yang H et al (2024) A process parameters decision approach considering spindle vibration in helical surface milling for minimising energy consumption and surface roughness value. J Brazilian Soc Mech Sci Eng 46:675. https://doi.org/10.1007/s40430-024-05242-w
31. Wu P, He Y, Li Y et al (2022) Multi-objective optimisation of machining process parameters using deep learning-based data-driven genetic algorithm and TOPSIS. J Manuf Syst 64:40–52. https://doi.org/10.1016/j.jmsy.2022.05.016
32. Sredanovic B, Cica D, Borojevic S et al (2024) Optimization of Superalloy inconel 718 micro-milling process by combined Taguchi and multi-criteria decision making method. J Brazilian Soc Mech Sci Eng 46:423. https://doi.org/10.1007/s40430-024-04996-7
33. Li S, Li S, Liu Z, Vladimirovich PA (2022) Roughness prediction model of milling noise-vibration-surface texture multi-dimensional feature fusion for N6 nickel metal. J Manuf Process 79:166–176. https://doi.org/10.1016/j.jmapro.2022.04.055
34. Montavon G, Müller K-R (2012) Big learning and deep neural networks. In: Montavon G, Orr GB, Müller K-R (eds) Neural networks: tricks of the trade: second edition. Springer Berlin Heidelberg, Berlin, Heidelberg, pp 419–420
35. Pashmforoush Farzad (2022) Mechanical properties prediction of various graphene reinforced nanocomposites using transfer learning-based deep neural network. Proceedings of the Institution of Mechanical Engineers, Part E: Journal of Process Mechanical Engineering 237:1214–1223. https://doi.org/10.1177/09544089221115306
36. Li B, Tian X, Zhang M (2022) Modeling and Multi-objective optimization method of machine tool energy consumption considering tool wear. Int J Precision Eng Manufacturing-Green Technol 9:127–141. https://doi.org/10.1007/s40684-021-00320-z
37. Paturi UMR, Yash A, Teja Palakurthy S, Reddy NS (2022) Modeling and optimization of machining parameters for minimizing surface roughness and tool wear during AISI 52100 steel dry

turning. Mater Today Proc 50:1164–1172. https://doi.org/10.1016/j.matpr.2021.08.047
38. Luan X, Zhang S, Li J et al (2018) Trade-off analysis of tool wear, machining quality and energy efficiency of alloy cast iron milling process. Procedia Manuf 26:383–393. https://doi.org/10.1016/j.promfg.2018.07.046
39. Bennett KS, DePaiva JM, Lazar E, Veldhuis SC (2024) Leveraging metaheuristic algorithms with improved hybrid prediction model framework for enhancing surface roughness optimization in CNC turning AISI 316. Int J Adv Manuf Technol 135:1955–1983. https://doi.org/10.1007/s00170-024-14654-w
40. Khamel S, Ouelaa N, Bouacha K (2012) Analysis and prediction of tool wear, surface roughness and cutting forces in hard turning with CBN tool. J Mech Sci Technol 26:3605–3616. https://doi.org/10.1007/s12206-012-0853-1
41. Nguyen V-H, Le T-T, Le MV et al (2023) Multi-objective optimization based on machine learning and non-dominated sorting genetic algorithm for surface roughness and tool wear in Ti6Al4V turning. Mach Sci Technol 27:380–421. https://doi.org/10.1080/10910344.2023.2235610
42. Işık AT, Çakıroğlu R, Günay M (2023) Multiresponse optimization of performance indicators through Taguchi-grey relational analysis in EDM of cemented carbide. CIRP J Manuf Sci Technol 41:490–500. https://doi.org/10.1016/j.cirpj.2023.01.012
43. Patel GCM, Jagadish (2021) Experimental modeling and optimization of surface quality and thrust forces in drilling of high-strength al 7075 alloy: CRITIC and meta-heuristic algorithms. J Brazilian Soc Mech Sci Eng 43:244. https://doi.org/10.1007/s40430-021-02928-3
44. Kong L, Zhuo X, Lei W et al (2025) Machining characteristics and optimization of TC4 alloy by mixed gas atomization discharge ablation milling (MA-DAM). J Manuf Process 133:11–24. https://doi.org/10.1016/j.jmapro.2024.11.046
45. St L, Wold S (1989) Analysis of variance (ANOVA). Chemometr Intell Lab Syst 6:259–272
46. Hou J, Zhou W, Duan H et al (2014) Influence of cutting speed on cutting force, flank temperature, and tool wear in end milling of Ti-6Al-4V alloy. Int J Adv Manuf Technol 70:1835–1845
47. Liu ZQ, Ai X, Zhang H et al (2002) Wear patterns and mechanisms of cutting tools in high-speed face milling. J Mater Process Technol 129:222–226
48. Lagarde Q, Wagner V, Dessein G, Harzallah M (2021) Effect of temperature on tool wear during milling of Ti64. J Manuf Sci Eng 143:071007
49. Luo H, Wang Y, Zhang P (2020) Effect of cutting parameters on machinability of 7075-T651 aluminum alloy in different processing methods. Int J Adv Manuf Technol 110:2035–2047
50. Sethupathy A, Shanmugasundaram N (2021) Prediction of cutting force based on machining parameters on AL7075-T6 aluminum alloy by response surface methodology in end milling. Materwiss Werksttech 52:879–890
51. Masmiati N, Sarhan AAD, Hassan MAN, Hamdi M (2016) Optimization of cutting conditions for minimum residual stress, cutting force and surface roughness in end milling of S50C medium carbon steel. Measurement 86:253–265
52. Pereira RBD, Leite RR, Alvim AC et al (2018) Multivariate robust modeling and optimization of cutting forces of the helical milling process of the aluminum alloy al 7075. Int J Adv Manuf Technol 95:2691–2715
53. Denkena B, Boehnke D, Dege JH (2008) Helical milling of CFRP–titanium layer compounds. CIRP J Manuf Sci Technol 1:64–69
54. Guo M, Ye Y, Jiang X, Wu C (2020) Comprehensive effect of multi-parameters on vibration in high-speed precision milling. Int J Adv Manuf Technol 108:2187–2195
55. Chen Y, Lu J, Deng Q et al (2022) Modeling study of milling force considering tool runout at different types of radial cutting depth. J Manuf Process 76:486–503
56. Li P, Zhang W (2014) Experiment based cutting force model for high speed milling of aluminium based composite. Mater Res Innovations 18:S5-35–S5-38. https://doi.org/10.1179/1432891714Z.000000000909
57. Chuangwen X, Jianming D, Yuzhen C et al (2018) The relationships between cutting parameters, tool wear, cutting force and vibration. Adv Mech Eng 10:1687814017750434. https://doi.org/10.1177/1687814017750434
58. Liu H, He Y, Mao X et al (2017) Effects of cutting conditions on excitation and dynamic stiffness in milling. Int J Adv Manuf Technol 91:813–822. https://doi.org/10.1007/s00170-016-9809-4
59. Arizmendi M, Campa FJ, Fernández J et al (2009) Model for surface topography prediction in peripheral milling considering tool vibration. CIRP Ann 58:93–96
60. Grossi N, Scippa A, Sallese L et al (2018) On the generation of chatter marks in peripheral milling: A spectral interpretation. Int J Mach Tools Manuf 133:31–46
61. Jiang H, Long X, Meng G (2008) Study of the correlation between surface generation and cutting vibrations in peripheral milling. J Mater Process Technol 208:229–238
62. Sheikhi MR, Gürgen S, Li J (2024) Vibration suppression and surface quality enhancement in milling thin-walled structures using shear thickening fluids. J Manuf Process 131:2219–2229
63. Surmann T, Biermann D (2008) The effect of tool vibrations on the flank surface created by peripheral milling. CIRP Ann 57:375–378
64. Liu G, Dang J, Li C et al (2019) Investigation on the vibration and machined surface quality in Tilt side milling of thin-walled plates. Int J Adv Manuf Technol 103:2287–2300
65. Ejiofor Matthew D, Shi J, Hou M, Cao H (2024) Improved STFT analysis using time-frequency masking for chatter detection in the milling process. Measurement 225:113899. https://doi.org/10.1016/j.measurement.2023.113899
66. Shi K, Zhang D, Ren J et al (2014) Multiobjective optimization of surface integrity in milling TB6 alloy based on Taguchi-Grey relational analysis. Adv Mech Eng 6:280313. https://doi.org/10.1155/2014/280313
67. Esme U (2014) Taguchi-Based grey relation optimization of machining parameters and cutting path strategies in CNC pocket milling operations. 56:741–747. https://doi.org/10.3139/120.110626
68. Sarıkaya M, Yılmaz V, Dilipak H (2015) Modeling and multi-response optimization of milling characteristics based on Taguchi and Gray relational analysis. Proc Inst Mech Eng B J Eng Manuf 230:1049–1065. https://doi.org/10.1177/0954405414565136
69. Jebaraj M, Pradeep Kumar M, Yuvaraj N, Mujibar Rahman G (2019) Experimental study of the influence of the process parameters in the milling of Al6082-T6 alloy. Mater Manuf Processes 34:1411–1427
70. Sur G, Motorcu AR, Nohutçu S (2022) Single and multi-objective optimization for cutting force and surface roughness in peripheral milling of Ti6Al4V using fixed and variable helix angle tools. J Manuf Process 80:529–545. https://doi.org/10.1016/j.jmapro.2022.06.016
71. Suneesh E, Sivapragash M (2021) Multi-response optimisation of micro-milling performance while machining a novel magnesium alloy and its alumina composites. Measurement 168:108345. https://doi.org/10.1016/j.measurement.2020.108345